DIGITAL LATCHING FERRITE

L-BAND PHASE SHIFTERS

DIGITAL LATCHING FERRITE L-BAND PHASE SHIFTERS

by

Mark S. Suthers, B.Eng.

A Thesis

Submitted to the Faculty of Graduate Studies

in Partial Fulfillment of the Requirements

for the Degree

Master of Engineering

McMaster University

November 1974

Master of Engineering (1974) McMaster University

(Electrical Engineering) Hamilton, Ontario

Title: Digital Latching Ferrite L-Band Phase Shifters

Author: Mark S. Suthers, B. Eng. (McMaster University)

Supervisor: Professor C.K. Campbell

Number of Pages: (x), 74

Scope and Contents:

Two prototype latching ferrite L-Band phase shifters were fabricated and their differential phase shifts were tested and compared. The theory of ferrite phase shifters is presented and the design equations to produce each phaser is developed.

ABSTRACT

The subject of this thesis is the design, fabrication and comparative testing of two protopype L-band ferrite digital latching phase shifters. One phaser is a variation of a design published by G.T. Roome and H.A. Hair, "Thin Ferrite Devices for Microwave Integrated Circuits", IEEE Trans. Microwave Theory Tech, vol. MTT-16 pp. 411-420, July 1968. The second design is original and is experimentally and theoretical compared to the first phaser. A comparative study was made because of technological difficulties in making these devices. Insertion losses of 2dB and an order of magnitude less than possible phase shift occured because of inadequate production facilities. Thus, the comparative study gave a common mode error to the published device and the new device.

Also, the theory of ferrite microwave phasers and a discussion of a particular system application which prompted this study are included in this thesis.

ACKNOWLEDGEMENTS

First and foremost, the author would like to thank Dr. C.K. Campbell who acted as supervisor to the study presented in this thesis. Dr. Campbell provided extensive amounts of valuable discussion time concerning the subjects of ferrites with respect to microwave applications. Also, the author would like to credit Dr. Campbell with a distinctive experimental approach in the pursuit of this engineering research.

Next, the author would like to thank Dr. S.S. Haykin and McMaster University for the use of the facilities of the Communications Research Laboratory. The author is also indebted to his colleagues in the CRL, namely: Mr. V. Crowe, Mr. P. Dupuis, Mr. M. El-Diwany, Mr. S. Ogletree, Mr. A. Patel and Mr. D. Seiler. Dr. W. Kinsner and Mr. P. Nolan also provided much helpful discussion.

Thirdly, the technical services provided by Mr. P. Edmonson, Mr. G. Innocente, and Mr. S. Kocsis were essential to the successful completion of this study. The quality of their work and the manner in which they completed the production tasks were very much appreciated.

Finally, the author thanks Miss. A. Hooker for her expert preparation of this manuscript.

TABLE OF CONTENTS

LIST OF FIGURES

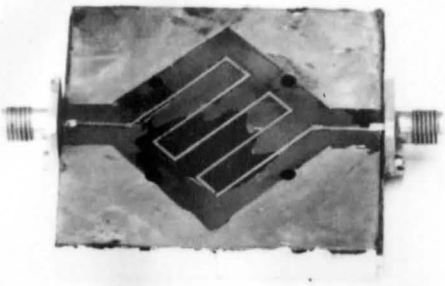

DOUBLE APERTURE PHASER

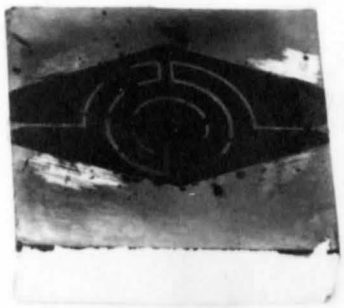

SINGLE APERTURE PHASER

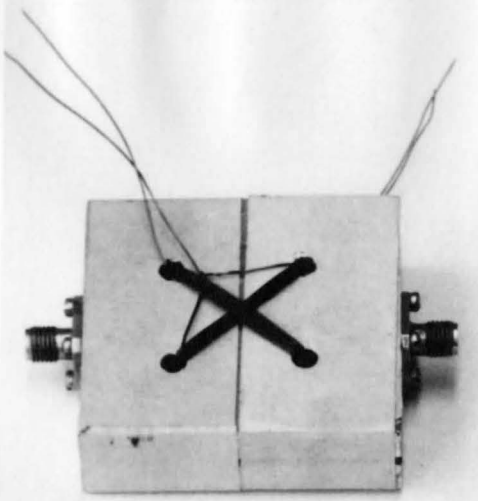

DOUBLE APERTURE PHASER

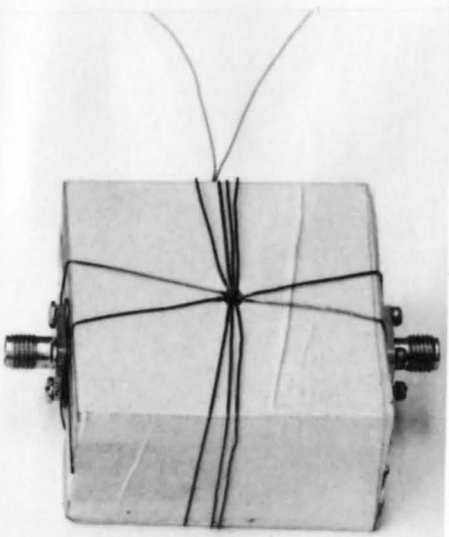

SINGLE APERTURE PHASER


8545A AUTOMATIC NETWORK ANALYZER
NETWORK ANALYSER SYSTEM
TELERAY 3300
RESEARCH INC

Chapter I

Introduction

1.1 Scope of Thesis:

The particular subject of this thesis is the design of a digital latching ferrite phase shifter in stripline configuration. The impetus for this investigation was provided by the Communications Research Centre in Ottawa. CRC is considering a linear phased array airborne communications system for the Atlantic commercial aircraft air traffic control system known as AEROSAT. The band of frequencies proposed for aircraft to satellite radio links will be in the 1.5 to 1.7 GHz band. These relatively long microwave lengths plus the size limitations set by CRC necessitated the use of a stripline configuration as will be demonstrated. (Reference [6])

Since this phase shifter may be incorporated into a linear phased array system, a brief discussion of the system requirements will be presented in the remainder of the first chapter. The general theory of how ferrite materials are used to produce a phase shift is presented in Chapter II. The actual design, testing and fabrication of prototype L-band phase shifters will make up the rest of the thesis.

1.2 Linear Phased Arrays:

The overall air traffic control system (ATCS) is shown diagramatically in Figure 1.1. The two satellites will be placed in synchronous orbits over the equatorial Atlantic region. Since the majority of commercial air traffic is north of the equator, the communications line of sight

between aircraft and satellite will significantly deviate from a vertical path. Also, since aircraft will fly from east to west as well as west to east, it is desireable to have a fan beam radiation system mounted on top of the aircraft. The fan beam allows one dimensional directivity from a single linear array for all aircraft orientations. The radiated energy is to be a right hand circularly polarized wave. The radiation pattern of the fan beam is to have 6dB ellipticity from 10^{o} above horizon to 10^{o} above horizon.

Assuming for the moment that quasi-isotopic radiators are available and refering to Figure 1.2, there are (n+1) isotropic radiating sources in a line. Adjacent elements are separated by a distance d and each sucessive element is fed out of phase by a phase factor α. The currents of the elements are related as $|I_i| = |I(n-i)|$ such that there is symmetry about the centre of the array. The radiated wave from each source is:

$$E_1 = A\, e^{-j(\beta r_1 + 0)}/r_1$$

$$E_2 = B\, e^{-j(\beta r_2 + \alpha)}/r_2$$

$$E_3 = C\, e^{-j(\beta r_3 + 2\alpha)}/r_3$$

$$\cdots\cdots$$

$$E_n = B\, e^{-j(\beta r_n + (n-1)\alpha)}/r_n$$

$$E_{n+1} = A\, e^{-j(\beta r_{n+1} + n\alpha)}/r_{n+1}$$

where $\beta = \omega\sqrt{\mu\varepsilon}$ is the propagation constant

α is the progressive phase shift

r_i is the distance from each element to the point of observation in the far field

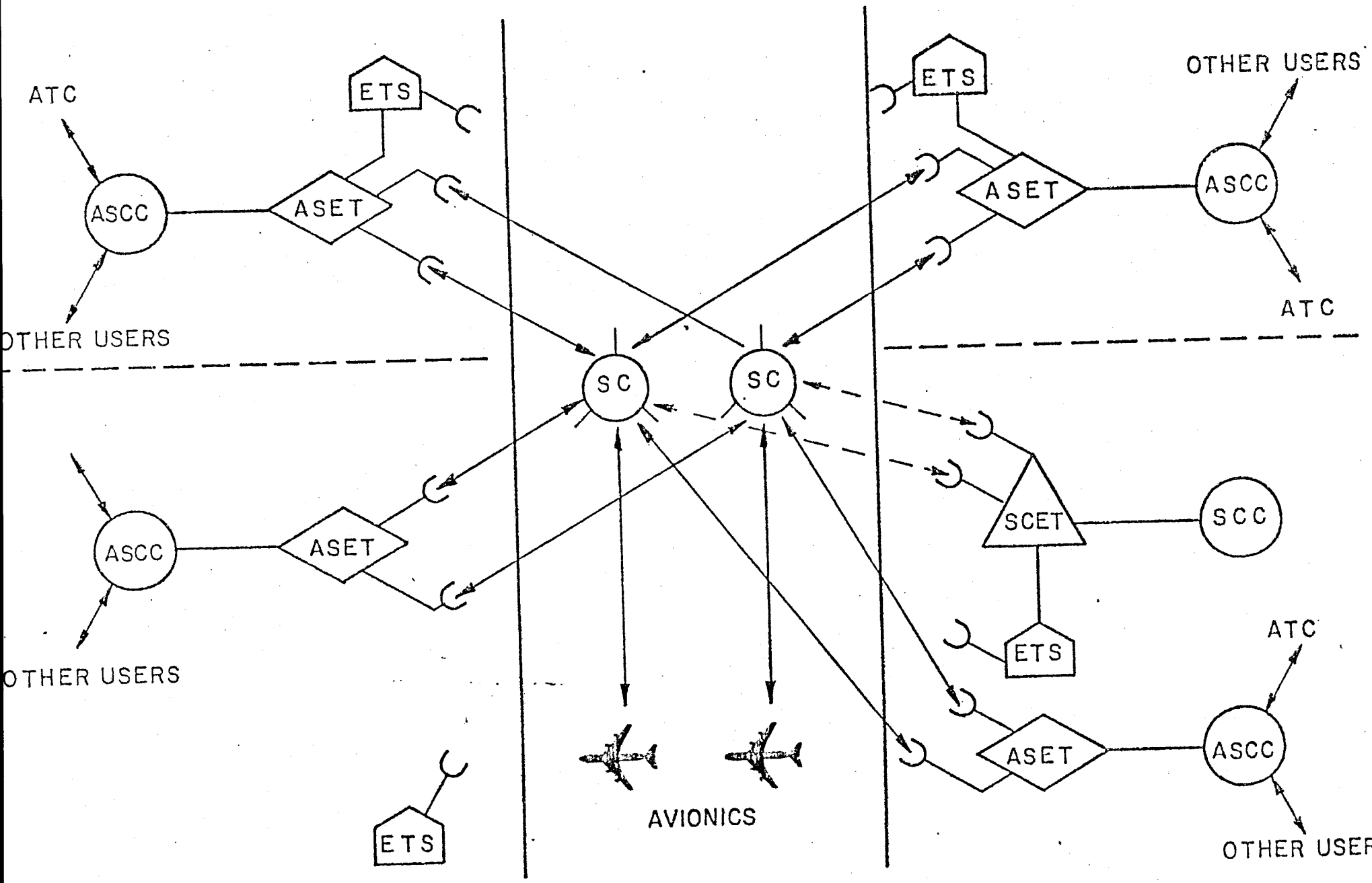

FIGURE 11- AEROSAT SYSTEM

A,B etc. are constant coefficients related to the E field due each element.

Assume for the present an odd number of elements. The far field of the array will be $E = \frac{Ae^{-j\beta r_1}}{r_1} + \frac{Be^{-j(\beta r_2+\alpha)}}{r_2} \ldots + \frac{Ae^{-j(\beta r_{n+1}+n\alpha)}}{r_{n+1}}$

For phase considerations

$$r_i = r_{n/2+1} - X_i \cos\theta$$

Refer to Figure 1.3

and for amplitude considerations

$$r_i \tilde{-} r_{n/2+1}$$

Putting $r_{n/2+1} = r_o$ gives:

$$E \tilde{-} \frac{e^{-j(\beta r_o+n/2\alpha)}}{r_o}\left[A_c e^{-j\frac{n}{2}(\beta d\cos\theta-\alpha)} + B_c e^{-j(\frac{n}{2}-1)(\beta d\cos\theta-\alpha)} + B_c e^{j(\frac{n}{2}-1)(\beta d\cos\theta-\alpha)}\right.$$

$$\left. + \ldots + A_c e^{j(\frac{n}{2})(\beta d\cos\theta-\alpha)}\right]$$

$$\tilde{-} \frac{e^{-j(\beta r_o+\frac{n}{2}\alpha)}}{r_o}\left[A\cos(\tfrac{n}{2})(\beta d\cos\theta-\alpha) + B\cos(\tfrac{n}{2}-1)(\beta d\cos\theta-\alpha) + C_{n/2}\cos(\beta d\cos\theta-\alpha)\right.$$

$$\left. + C_{n/2+1}\right]$$

Grouping the constants gives

$$E = E_o + E_1\cos(\beta d\cos\theta-\alpha) + \ldots + E_{\frac{n}{2}}\cos(\tfrac{n}{2}-1)(\beta d\cos\theta-\alpha) + E_{\frac{n}{2}+1}\cos(\tfrac{n}{2})(\beta d\cos\theta-\alpha)$$

This is easily recognized as a truncated Fourier series. In the case of an even number of elements a similar derivation gives a similar result. If the magnitudes of all the coefficients of the terms are equal, then the radiation pattern of the θ-z plane is the familiar sinc function. The side lobes may be reduced at the expense of main beam broadening by choosing a binomial, Chebyshev or elliptic relationship between the

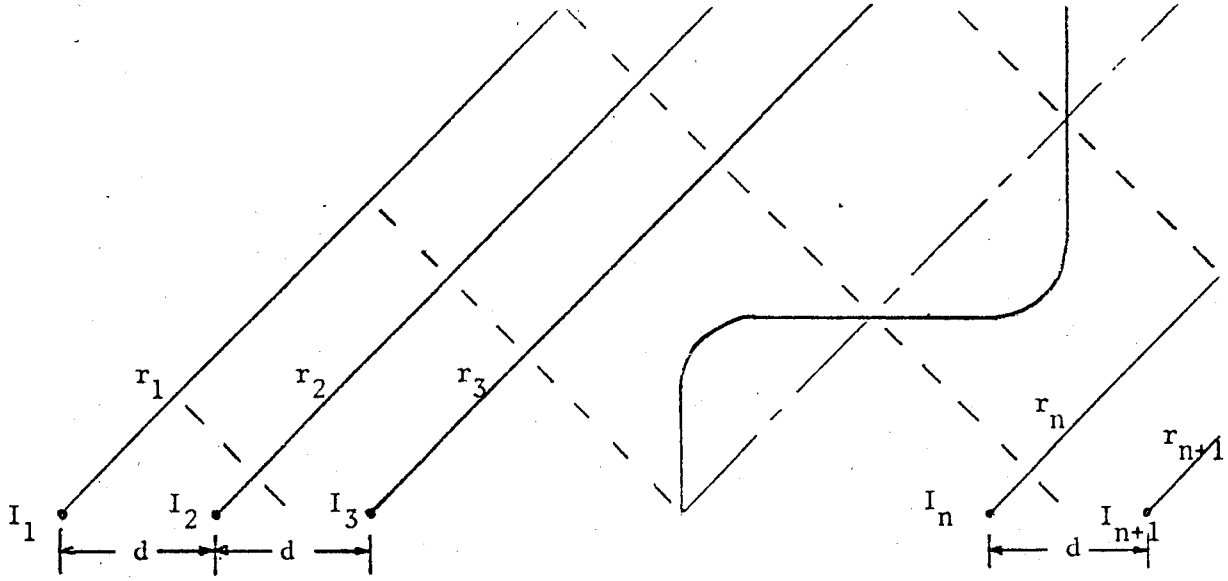

Figure 1.2 Linear array of n+1 isotropic sources

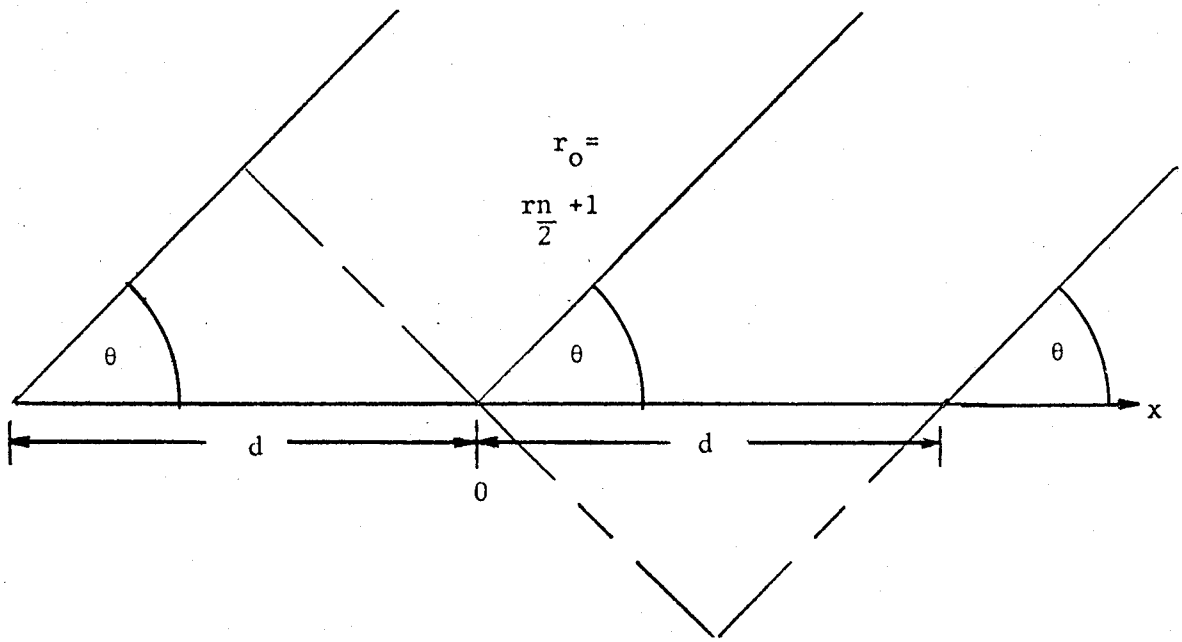

Figure 1.3 Geometry of linear phased array of n+1=3 isotropic radiating sources.

antenna currents. These polynomial relationships give spatial antenna patterns that when transformed from polar to rectangular coordinates are the familiar binomial, Chebyshev and elliptic plots. A more extensive treatment of this subject is found in many texts on EM Theory such as Reference [1].

1.3 Antenna Elements:

The above array mathematics used the concept of an isotropic radiating element. For the AEROSAT system, a uniform radiation pattern for $0 < \theta \leq 180^{o}$ is required, thus it is necessary that each element produce such a pattern within 3dB ellipticity bounds (because of RHCP wave, two elements are required to produce a unit array element, thus, the error criterion will be 3 dB for x axis element plus 3 dB for y axis element giving 6 dB elipticity which is CRC's specification).

An array of isotropic sources produces a conical pattern about the axis of the array. By placing the array elements above a ground plane, the radiated energy is restricted to the hemisphere above the ground plane. The resulting pattern may be obtained by replacing the ground plane by image sources symmetrically about the ground plane as described in Reference [1]. If the driving point of the radiating elements is above the ground plane, then the effect of the ground plane is to produce a two dimensional array. This adds to the complexity of adjusting the phase between elements when switching the beam angle. Since the array is to be mounted on the upper part of the aircraft fuselage; it is not possible to eliminate the ground plane, thus it is desirable to place the driving point of the antenna

element at the ground plane.

To produce the broad beam width, CRC has suggested crossed drooping dipoles fed 90^{o} out of phase be used for each array element. By drooping the dipole, the polar pattern of the dipole will be distorted so as to produce the desired broad beam. By crossing two of these drooping dipoles and feeding them 90^{o} out of phase the RHCP wave may be produced. While this system is feasible, it is possible to improve the design by using a bent monopole at two array points instead of crossed dipoles at a single point.

By using a monopole, the driving point is at the ground plane thus the array remains linear with the ground plane in place as pointed out before. Also by using a monopole, it is not necessary to balance the currents in each half of a dipole. Since the driving circuitry is in strip line configuration, it would be necessary to employ a balun between the phase shifting networks and the radiating dipoles elements if the currents are to be balanced.

By using image theory, it is easy to see that a bent monopole over a groundplane appears in the far field as a vertically oriented drooping dipole. This is illustrated in Figure 1.4. Also assuming the monopole is approximately a quarter wave length long, the height of the radiating element profile will be approximately one eighth of a wavelength. This is a space saving feature which is of concern with CRC specifications of a maximum of 0.6 λ height for the array. (Reference[6])

The last point of consideration of antenna elements is that of separating the two 90^{o} phase separated radiating elements that produce the

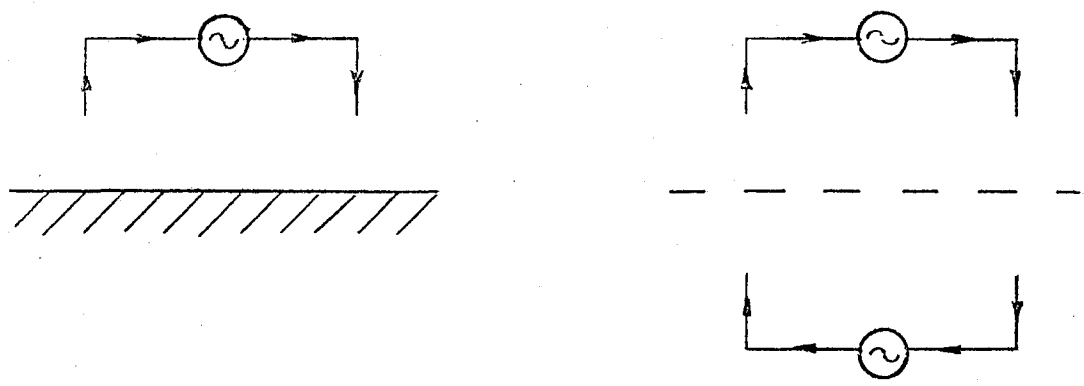

Figure 1.4a Equivalent image of drooping dipole over ground plane.

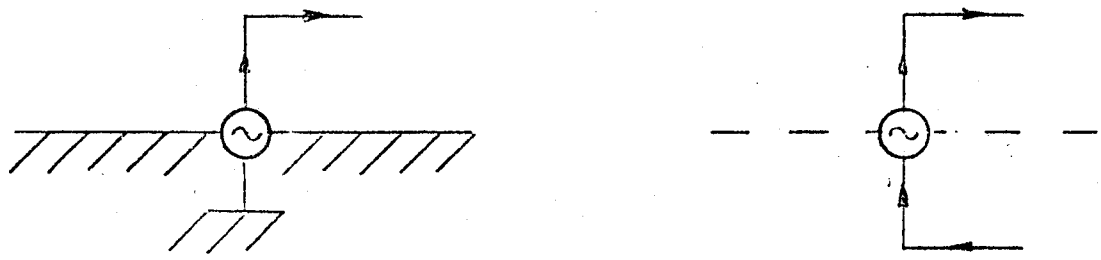

Figure 1.4b Equivalent image of bent monopole over ground plane.

RHCP wave. If the two elements are separated with the appropriate phasing, a RHCP wave may be produced. The advantages of doing this is that a single semi isotropic source (crossed drooping dipoles for instance) now becomes a two element array. This in effect cuts the required number of elements to produce a given directivity in half. The real advantage found in this concept is that the radiating elements may now be integrated in MIC form along with phasing components in a single planar module for each array element position. This offers an obvious cost advantage in any production run.

The splitting of the crossed elements into two array positions is shown in Figure 1.5. The portions of each element that are active in producing RHCP are also tabulated in Figure 1.5

1.4 Phase Shifters:

To produce the varying discrete steps in phase shift between elements, it is necessary to control the phase of the individual current sources for each element or to use a common source and vary the electrical length to each antenna element from the power divider. The latter solution so far is the easier of the two to implement. Generally, there are three techniques to vary the electrical length which are:

(1) PIN diode phasers

(2) Butler matrix array

(3) Ferrite phasers.

The PIN diode phasors exist in a variety of configurations but all operate on the principle of creating a short circuit at various points on the

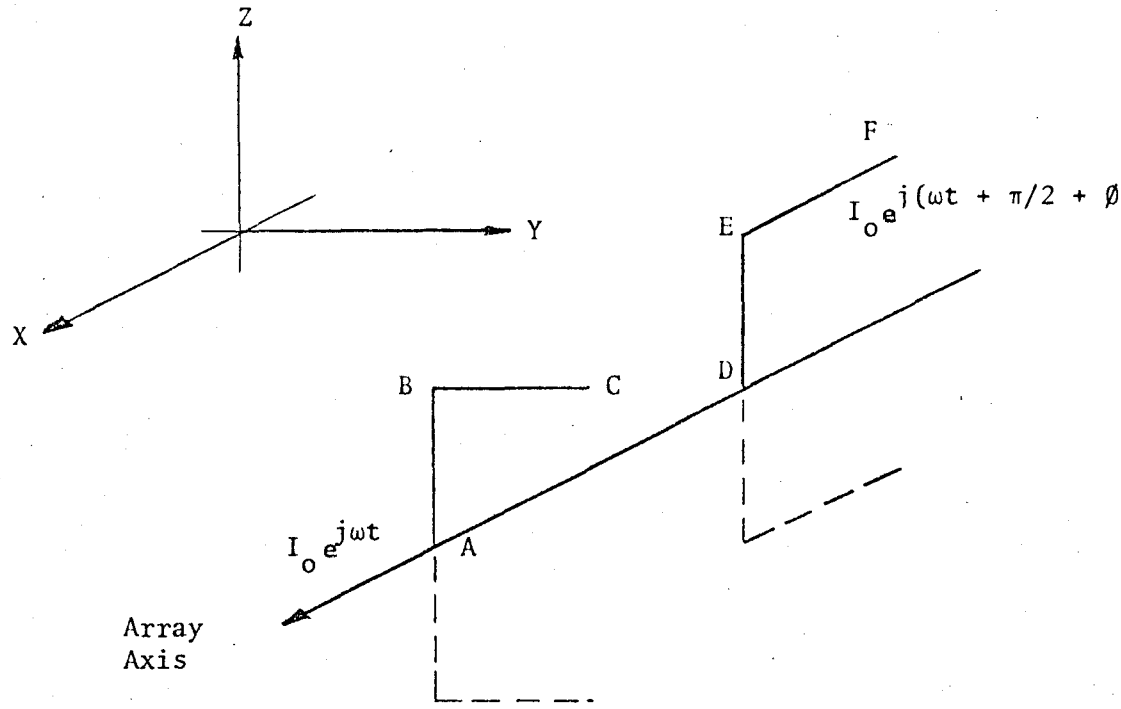

X Axis:	Section BC + Section ED	RHCP
Y Axis:	Section AB + Section EF	RHCP
Z Axis:	Section BC + Section EF	RHCP

Figure 1.5: Splitting crossed phased elements into two array points

transmission line. The reflection from these shorts will vary in phase proportionally to the distance from the inport to the short plus the distance from the short to the outport. An extensive treatment of this subject exists in the literature and is beyond the scope of this thesis.

The Butler matrix array consists of a tree of 3dB couplers. By switching the inputs from A to B to C to D in Figure 1.6, the output phases are retarded by differing discrete amounts as shown in Figure 1.6. By placing appropriate phase lengths in between couplers, a coherent progressive phase shift may be obtained.

Ferrite phase shifters are based on a perturbation of transmission line parameters. By changing the DC magnetic field applied to the ferrite dielectric substrate through which the EM wave is guided, the effective permeability seen by the r.f. field is changed. This results in a change in propagation velocity and thus appears as a phase shift through the two port device. There is a wide variety of phasers employing ferrite technology. Most of these devices are employed in wave guide systems while a few planar devices have been designed.

A final consideration specified by CRC is that the array is to be operational within the environmental extremes of $\pm$ 50^{o}C for subsonic aircraft and -50^{o} to +150^{o}C for supersonic aircraft. It is known that ferrite materials are quite temperature dependent as seen in the specification sheet for the material used in this thesis. Environmental testing and temperature controlling techniques were not investigated in this thesis, since these are system engineering problems and this thesis is concerned with device design.

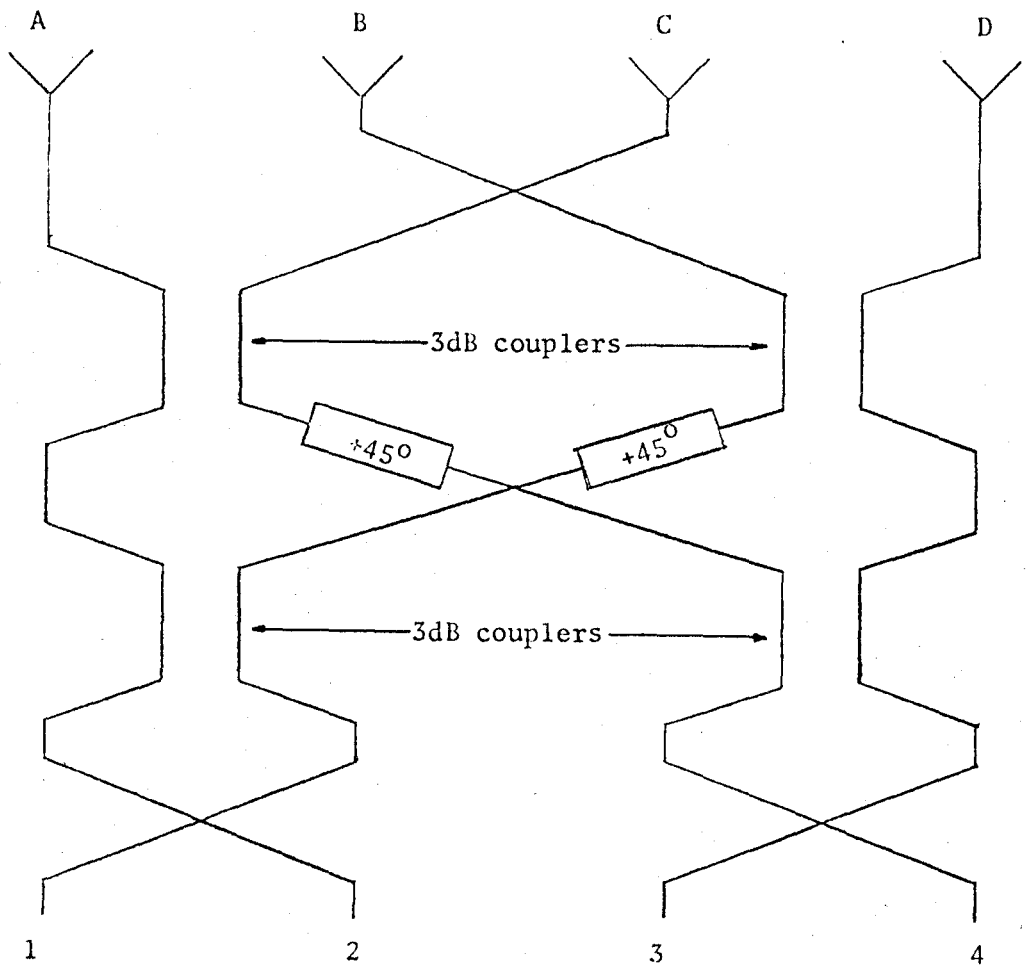

	A	B	C	D	
1	$-\frac{2\pi}{4}-\frac{8\pi}{4}$ $=-\frac{10\pi}{4}$	$\frac{\pi}{4}-\frac{8\pi}{4}$ $=-\frac{7\pi}{4}$	$\frac{-4\pi}{4}$	$\frac{-3\pi}{4}$	$\frac{-3\pi}{4}$
2	0	$-\pi/4$	$\frac{-2\pi}{4}$	$\frac{-3\pi}{21}$	$\frac{-\pi}{4}$
3	$-3\pi/4$	$-2\pi/4$	$-\pi/4$	0	$+\pi/4$
4	$-\pi/4$	$-4\pi/4$	$\pi/4-3\pi/4$ $=-\frac{7\pi}{4}$	$\frac{-2\pi}{4}-\frac{3\pi}{4}$ $=\frac{-10\pi}{4}$	$+\frac{3\pi}{4}$

Figure 1.6: Four state Butler matrix.

The subject of this thesis is the design, testing and comparison of two planar digital latching ferrite phasers.

General overviews of recent advances in phase shifters at microwave frequencies are found in References [8], [9] and [10].

Explanations of Butler matricies may be found in Reference [11].

Extensive treatments of ferrite phaser theory and device descriptions are to be found in the classical Reference [12] and in Reference [13].

Chapter II

Theory of Ferrite Phase Shifters

2.1 General:

The literature on the theory of ferrite phase shifters is at best vague in its description of how the actual phase shift occurs. Part of the reason for this problem is that to a large extent, the actual physical mechanisms involved are not fully understood. Because of this, the author will attempt in this chapter to present a relatively simplistic description of the physical mechanisms involved in the production of the observed phase shift in the devices described in this thesis.

2.2 Unit Magnetic Dipole:

Consider the simplest atomic structure of a hydrogen atom as the basic system . A single electron orbits about the nucleus thus producing an effective circular current which results in a magnetic flux through the current loop. The electron also spins about its own axis which may be thought of as a distributed current flow about the spin axis. It is the magnetic field due to this spin that is considered to be the primary source of magnetic flux from a single electron's motion. For general theory considerations, consider the magnetic flux in a magnetic material to be primarily due to electron spin. (Reference [2])

Considering a cubic structure of dipoles as in Figure 2.1, there is effectively a circular current flow at each lattice point. Having a large DC magnetic field as shown in Figure 2.1, then the circular current at each lattice point will tend to align itself with the applied D.C. field.

If a small magnetic field (say due to a propagating r.f. field) is applied at right angles to the D.C. field, the current loop will feel a torque as shown in Figure 2.1 and thus the magnetic moment μ of the magnetic dipole will tend to move to some angle θ with $\vec{B}_{DC}$ as shown in Figure 2.2. Since the spinning electron has mass, it is gyrotropic in nature and having been disturbed from its equilibrium axis, it will tend to precess about the $H_o(B_{DC})$ axis at some natural resonant frequency which is a function of $\overline{H}_o$ and the angular momentum $\overline{J}$ of the electron. If the $h_{rf}=\mu\, b_{rf}$ alternates at the same resonant frequency, then the precession grows in amplitude and absorbs energy from the applied r.f. field.

The relationship between μ and $\overline{J}$ has been found to be:

$$\frac{\nu}{J} = \gamma = -2.21 \times 10^5 \frac{\text{rad/sec}}{\text{At/m}} \qquad (2.1)$$

in the rationalized MKS system of units. Unfortunately, ferrite technology has evolved in c.g.s. units where:

$$\gamma = -2.8 \text{ Mhz/Oersted}$$

Consider Figure 2.2 where $\boldsymbol{\nu}$ has been disturbed from $\theta=0$. The magnetic dipole $\boldsymbol{\nu}$ is acted upon primarily by H_o, thus the torque exerted on $\boldsymbol{\nu}$ by H_o is given by:

$$\overline{T} = \overline{\nu} \times \overline{H_o} \qquad 2.2$$

It is known that:

$$\overline{J} = \gamma^{-1}\, \overline{\nu}$$

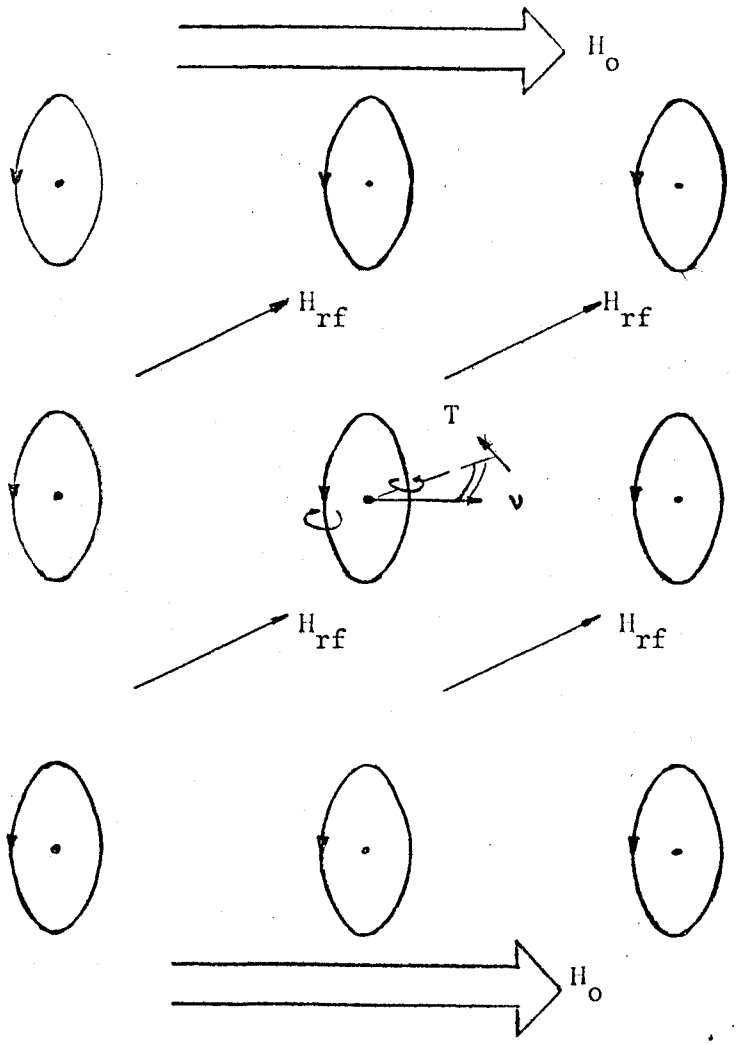

Figure 2.1: Cubic magnetic dipole structure under influence of H_o(DC) and H_{rf}

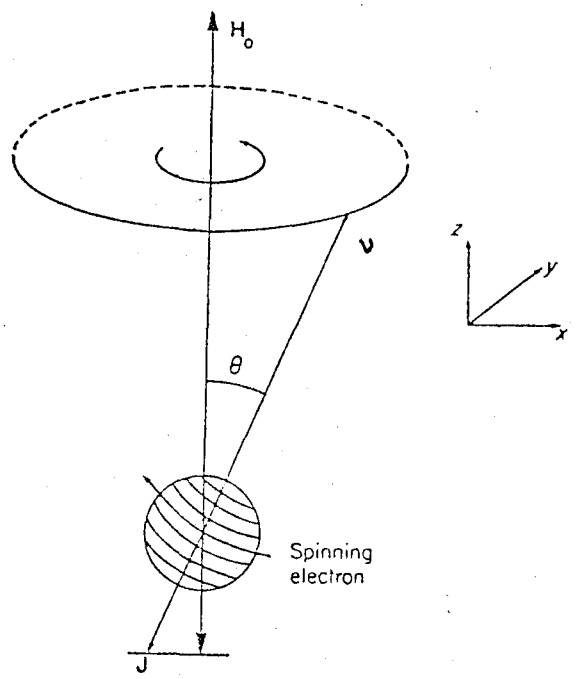

Figure 2.2: Magnetic moment precession about a static magnetic field

and also $\overline{T} = d\overline{J}/dt$

thus $$T = \frac{1}{\gamma} \frac{d\overline{\nu}}{dt} \qquad 2.3$$

By equating 2.2 and 2.3:

$$\frac{d\overline{\mu}}{dt} = \gamma \ (\overline{\nu} \times \overline{H}_o) \qquad 2.4$$

which is the equation of motion for a single magnetic dipole.

2.3 Equation of Motion:

The total effective magnetization is given by $\overline{M}_o = N \overline{\nu}$ where N is the total number of unbalanced electron spins (unit magnetic dipole) per unit volume of material. Thus the equation of motion for the solid is:

$$\frac{d \overline{M}_o}{d t} = \gamma \ (\overline{M}_o \times \overline{H}_o) \qquad 2.5$$

In an infinite ferrite medium that is magnetized, consider the tensors:

$\overline{H} = \overline{H_o} + \overline{h}$ and $\overline{M} = \overline{M_o} + \overline{m}$

where

$$\overline{H_o} = \begin{bmatrix} 0 \\ 0 \\ H_o \end{bmatrix} \qquad \overline{h} = \begin{bmatrix} h_x \\ h_y \\ h_z \end{bmatrix}$$

$$\overline{M_o} = \begin{bmatrix} 0 \\ 0 \\ M_o \end{bmatrix} \qquad \overline{m} = \begin{bmatrix} m_x \\ m_y \\ m_z \end{bmatrix}$$

As developed in Reference [3] using equation 2.5, the above magnetic state gives:

$$\ddot{m}_x + \omega_o^2 m_x = \mu_o \omega_m \omega_o h_x - \mu_o \omega_m \dot{h}_y$$

$$\ddot{m}_y + \omega_o^2 m_y = \mu_o \omega_m \dot{h}_x + \mu_o \omega_m \omega_o h_y \qquad 2.6$$

$$m_z = 0$$

where $\omega_m = -\frac{\gamma M_o}{\mu_o}$ 2.6a

and $\omega_o = -\gamma H_o$ 2.6b

If the r.f. quantities (lower case) are of the form $e^{j\omega t}$, then the equations of 2.6 become:

$$(-\omega^2 + \omega_o^2)\, m_x = \mu_o \omega_m \omega_o h_x - j\mu_o \omega_m \omega h_y$$

$$(-\omega^2 + \omega_o^2)\, m_y = -j\mu_o \omega_m \omega h_x + \mu_o \omega_m \omega_o h_y$$

$$m_z \tilde{=} 0$$

which in tensor form gives:

$$\begin{bmatrix} m_x \\ m_y \\ m_z \end{bmatrix} \begin{bmatrix} \frac{\mu_o \omega_m \omega_o}{\omega_o^2 - \omega^2} & -j\frac{\mu_o \omega_m \omega}{\omega_o^2 - \omega^2} & 0 \\ \frac{\mu_o \omega_m \omega}{\omega_o^2 - \omega^2} & \frac{\mu_o \omega_m \omega_o}{\omega_o^2 - \omega^2} & 0 \\ 0 & 0 & 0 \end{bmatrix} \begin{bmatrix} h_x \\ h_y \\ h_z \end{bmatrix}$$

$$= \mu_o \begin{bmatrix} \chi_{xx} & \chi_{xy} & 0 \\ \chi_{yx} & \chi_{yy} & 0 \\ 0 & 0 & 0 \end{bmatrix} \begin{bmatrix} h_x \\ h_y \\ h_z \end{bmatrix} \qquad 2.7$$

where:

$$\chi_{xx} = \chi_{yy} = \frac{\omega_m \omega_o}{\omega_o^2 - \omega^2}$$

$$\chi_{yx} = -\chi_{xy} = j \frac{\omega_m \omega}{\omega_o^2 - \omega^2}$$

2.4 Polder Permeability Tensor:

The above χ's are components of the susceptibility tensor that have singularities at an angular frequency ω_o which is known as the resonance condition.

Recall the definition $\omega_o = -\gamma H_o$ and note that the susceptibility tends to approach infinity when the r.f. frequency approaches ω_o. Thus the applied magnetic field intensity determines the resonant frequency. The tensor permeability is related to the susceptibility tensor by:

$$[\mu_r] = [I] + [\chi] \qquad 2.7$$

where $[I]$ is the identity matrix.

since $\bar{b} = \mu_o \bar{h} + \bar{m}$ or $\bar{b} = \mu_o [\mu_r] \bar{h}$

where

$$[\mu_r] = \begin{bmatrix} \mu & -jk & 0 \\ jk & \mu & 0 \\ 0 & 0 & 1 \end{bmatrix} \qquad 2.8$$

and

$$\mu = 1 + \chi_{xx}$$

$$jk = -\chi_{xy}$$

Equation 2.8 is the well known Polder tensor permeability. Since the susceptibility approaches infinity as $\omega \to \omega_o$, so also do the permeability

tensor elements, μ and k. However, since an infinite magnetic flux is unnatural, a loss mechanism must occur if the mathematics is to be valid.

2.5 Effective Permeability of Linear Polarized Wave in Ferrite Medium:

In the system considered above, the applied H_o field was along the z axis which was the direction of propagation of the r.f. energy. Consider the $E_{r.f.}$ field to be $\hat{y}$ polarized in a ferrite medium separated by a guiding structure of two parallel conducting plates as shown in Figure 2.3. At the conducting boundaries of $y = \pm a$, it is known that no E field tangent to a conductor may exist; that is $E_x(y=\pm a)=0$. Because of this there may be no Faraday rotation of the wave as it propagates along the z axis. If there were, then at some point, for example, the resultant E field would be in the $\hat{x}$ direction completely, resulting in a E_{tan} at $y = \pm a$ which is physically impossible. Keeping this in mind recall Maxwell's curl $\bar{E}$ equation:

$$\nabla \times \bar{E} = -j\omega \mu_o [\mu_r] \bar{h}$$

It is known that $E_z = 0$ $\qquad$ $E_x = 0$

$$\frac{\partial}{\partial x} = 0 \qquad \frac{\partial}{\partial y} = 0$$

Thus:

$$\begin{bmatrix} -\frac{\partial E_y}{\partial z} \\ 0 \\ 0 \end{bmatrix} = j\omega\mu o \begin{bmatrix} \mu & -jk & 0 \\ jk & \mu & 0 \\ 0 & 0 & 1 \end{bmatrix} \begin{bmatrix} h_x \\ h_y \\ h_z \end{bmatrix}$$

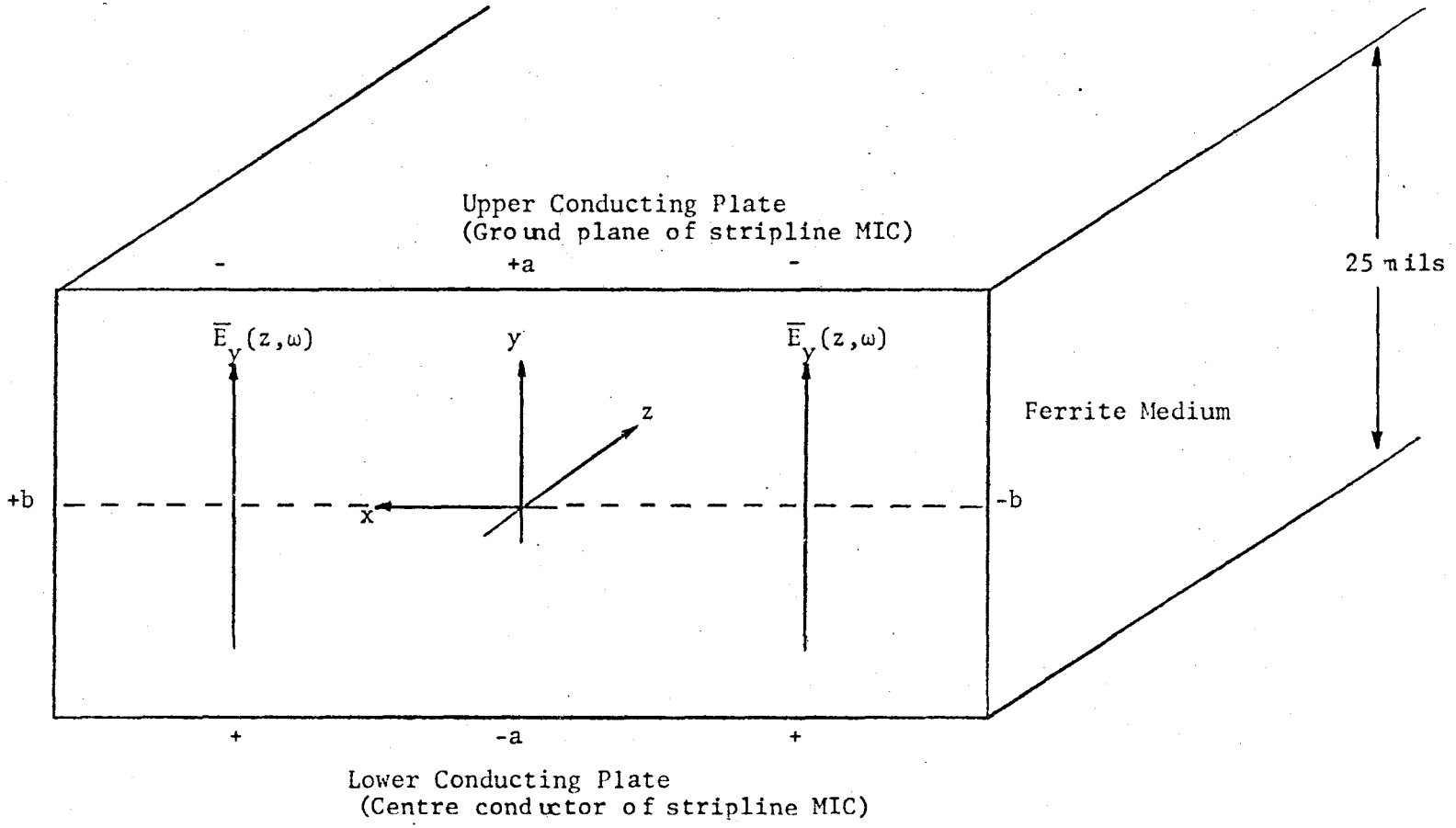

Figure 2.3: Parallel conducting plate guiding structure separated by ferrite medium. (this approximates 1/2 of a stripline MIC structure neglecting edge effects. The bottom 1/2 is a reflection of the fields shown in the above diagram.)

Taking $$E_y = E_o e^{-j\beta z}$$

then $$\frac{\partial E_y}{\partial z} = -j\beta E_y$$

Substituting this into Equation 2.9 gives:

$$j\beta \begin{bmatrix} E_y \\ 0 \\ 0 \end{bmatrix} = j\omega\mu o \begin{bmatrix} \mu & -jk & 0 \\ jk & \mu & 0 \\ 0 & 0 & 1 \end{bmatrix} \begin{bmatrix} h_x \\ h_y \\ h_z \end{bmatrix} \qquad 2.10$$

Since only the electrical boundary conditions are known and only E_y exists, it is necessary to put $\bar{h}$ in terms of E_y to find the effective permeability μ_e. Rearranging Equation 2.10 gives:

$$\begin{bmatrix} h_x \\ h_y \\ h_z \end{bmatrix} = \frac{\beta}{\omega\mu_o} [\mu_r]^{-1} \begin{bmatrix} -E_y \\ 0 \\ 0 \end{bmatrix} \qquad 2.11$$

Taking the inverse of $[\mu_r]$ gives:

$$[\mu_r]^{-1} = \frac{1}{\mu^2-k^2} \begin{bmatrix} \mu & jk & 0 \\ -jk & \mu & 0 \\ 0 & 0 & \mu^2-k^2 \end{bmatrix} \qquad 2.12$$

Thus

$$\left.\begin{aligned} h_x &= -\frac{\beta}{\omega\mu_o}\left(\frac{\mu}{\mu^2-k^2}\right) E_y \\ h_y &= \frac{\beta}{\omega\mu_o}\left(\frac{jk}{\mu^2-k^2}\right) E_y \\ h_z &= 0 \end{aligned}\right\} \qquad 2.13$$

It is known that for a plane linear wave:

$$h_x = -\eta^{-1} E_y$$

thus

$$\eta^{-1} = \frac{\beta}{\omega\mu_o} \left(\frac{\mu}{\mu^2 - k^2} \right)$$

which gives the resulting effective permeability $\mu_e = \frac{\mu^2 - k^2}{\mu}$ 2.14

Substituting for μ and k gives:

$$\mu_e = 1 + \frac{\mu_o \omega_m \omega_o}{\omega_o^2 - \omega^2} - \frac{\mu_o^2 \omega_m^2 \omega^2}{\omega_o^2 - \omega^2 + \mu_o \omega_m \omega_o} \qquad 2.16$$

If the applied H_o field were changed to the $\hat{x}$ direction, then the permeability tensor will be:

$$[\mu_r] = \begin{bmatrix} 1 & 0 & 0 \\ 0 & \mu & -jk \\ 0 & jk & \mu \end{bmatrix} \qquad 2.17$$

Taking $\nabla \times \bar{E} = -j\omega \mu o [\mu_r] \bar{h}$ as before gives:

$$[\mu_r]^{-1} = \begin{bmatrix} 1 & & 0 \\ 0 & \frac{\mu}{\mu^2 - k^2} & \frac{jk}{\mu^2 - k^2} \\ 0 & \frac{-jk}{\mu^2 - k^2} & \frac{\mu}{\mu^2 - k^2} \end{bmatrix}$$

Thus

$$\left.\begin{aligned} h_x &= -\frac{\beta}{\omega\mu_o} E_y \\ h_y &= 0 \\ h_z &= 0 \end{aligned}\right\} \qquad 2.19$$

The effective permeability seen by the propagating r.f. wave is that for free space.

2.6 Phase Shifters:

By changing the D.C. magnetic field's direction, the effective relative permeability has been changed from: $\mu_e = \frac{\mu^2 - k^2}{\mu}$

$$\text{to:} \quad \mu_e = 1$$

It is this principle that is used in many ferrite phase shifters. As noted previously $h_x = -\eta^{-1} E_y$ where $\eta = \left(\frac{\mu_x \mu_o}{\varepsilon_y \varepsilon_o} \right)^{1/2}$

Denote

$$\mu_{\parallel} = \mu_o \left(\frac{\mu^2 - k^2}{\mu} \right) \qquad 2.21$$

as the longitudinal magnetization which is parallel to the r.f. propogation direction and : $\mu_{\perp} = \mu_o$ 2.22

as the transverse magnetization which is at right angles to the direction of r.f. propagation.

It is known that $\beta = \omega(\mu_o \varepsilon_o \varepsilon_y \mu_x)^{1/2}$ thus continuing the above subscript convention: $\beta_{\parallel} = \omega(\mu_o \varepsilon_o \varepsilon_y)^{1/2} \left(\frac{\mu^2 - k^2}{\mu} \right)^{1/2}$ 2.23

and $\beta_{\perp} = \omega(\mu_o \varepsilon_o \varepsilon_y)^{1/2}$ 2.24

The difference between these two quantities is:

$$\Delta\beta = \beta_{\perp} - \beta_{\parallel} = \omega(\mu_o \varepsilon_o \varepsilon_y)^{1/2} \left[1 - \left(\frac{\mu^2 - k^2}{\mu} \right)^{1/2} \right]$$

For materials and frequencies of interest $|k| << |\mu|$ thus:

$$\Delta\beta \simeq \omega(\mu_o \varepsilon_o \varepsilon_y) \left(\frac{1}{2} \frac{k^2}{\mu^2} \right) \qquad 2.25$$

It is possible to determine the differential phase shift between the two remanent states of a phaser by using equation 2.25 if the total electrical length in transverse wave lengths ($\lambda_\perp$) is known. Obviously only those portions of the line in a given device that experience both states may be included in the total. One reason for choosing a frequency such that $|k|<<|\mu|$ (aside from loss considerations) is that the difference in characteristic impedance of the medium in the two different magnetized states causes a reflection of incident power at each port due to impedance mismatch. It is easy to see that:

$$z_{\parallel} = z_\perp \left(\frac{\mu^2-k^2}{\mu} \right)^{1/2}$$

$$\tilde{-} z_\perp \left(1 - \frac{1}{2} \frac{k^2}{\mu^2} \right) \qquad 2.26$$

If the impedances $z_{\parallel}$ and $z_\perp$ are chosen such that $z_o = \frac{1}{2}(z_\perp + z_{\parallel})$ where z_o is the impedance of the circuitry connected to the device, then approximately equal power will be reflected in either state thus

$$z_\perp \tilde{-} \frac{4\mu^2 z_o}{4\mu^2 - k^2} \qquad 2.28a$$

Since $z_{\parallel} < z_o$ and $z_\perp > z_o$, then the power reflected from $z_{\parallel}$ is slightly higher than that reflected from $z_\perp$. The optimization is theoretically quite feasible but because the theory is not very exact, the effort is not really justified. Normally, frequencies are chosen such that, power reflections and transmission losses are less than 1/2 dB. On this basis, equation 2.28 is a valid starting point from an engineering point of view. The reflection coeficient offered by 2.28a is:

$$\Gamma_{\perp} = \frac{k^2}{8\mu^2 - k^2} \qquad 2.29a$$

and that offered by equation 2.28b is:

$$\Gamma_{\parallel} = \frac{-3k^2}{8\mu^2 - 3k^2} \qquad 2.29b$$

These equations will be design equations if very low reflection coefficients are required.

2.7 Transmission Losses:

In most designs, the principal consideration will be to obtain the maximum phase shift per unit length of transmission line without incurring any significant losses. Assuming operation above resonance, the losses and the differential phase shift vary proportionally as ω_r/ω i.e. as $\omega_r/\omega \to 0$, so also do the losses and $\Delta\beta$. The losses are due to two phenomena: (1) reflection of incident power due to impedance mismatch and (2) transmission losses. In the majority of cases, the lowest usable frequency for a given material will be determined by the transmission losses. In reference [4], page 8, the relationship: $\alpha\,\omega = \frac{\gamma\,\Delta H}{2}$ 2.30 is derived where: α is the damping factor

ω is the angular frequency at which the line width is specified for the given material

γ is the gyromagnetic ratio

ΔH is the 3dB line width of the material at ω

As previously noted, the ferrite technology has evolved in c.g.s. units. Thus in c.g.s.

equation (2.30) becomes:

$$\alpha = \frac{\gamma \, \Delta H}{2 f_s} \qquad 2.31$$

where $\gamma = -2.8$ MHz/Oe.

ΔH = 3dB linewidth in Oe at f_s

f_s = frequency in MHz specified for ΔH

Note that for $\omega_o < \omega_m$, α is a negative number.

In physical terms, α is a dimensionless quantity that accounts for the mainly phonon loss mechanisms that occur near resonance. In the vicinity of the resonant frequency, energy from the r.f. field produces the precession of magnetic dipoles as previously described. This motion tends to produce lattice vibrations and other sorts of magnetic and mechanical motion such as domain wall movements. Not all the energy is returned to the electrical form as some escapes in the form of these phonon losses that eventually become heat losses. This consideration is obviously very important for high power devices. The term α is defined in [3] page 6 as an imaginary frequency term such that:

$$\chi_{xx} = \chi_{yy} = \frac{\omega_m(\omega_o + j\omega\alpha)}{(\omega_o + j\omega\alpha)^2 - \omega^2} \qquad 2.32$$

and

$$\chi_{yx} = -\chi_{xy} = \frac{j\omega_m\omega}{(\omega_o + j\omega\alpha)^2 - \omega^2} \qquad 2.33$$

Thus if α is small as it will be for materials and frequencies of interest, then:

$$\mu \simeq 1 + \frac{\omega_m(\omega_o + j\omega\alpha)}{\omega_o^2 - \omega^2}$$

$$\mu' - j\mu'' = \left(\frac{\omega_o^2 - \omega^2 + \omega_m \omega_o}{\omega_o^2 - \omega^2} \right) - j\left(- \frac{\omega_m \omega \alpha}{\omega_o^2 - \omega^2} \right) \qquad 2.34$$

and $$jK \tilde{=} j \frac{\omega_m \omega}{\omega_o^2 - \omega^2}$$

$$j(K' - jK'') \tilde{=} j\left(\frac{\omega_m \omega}{\omega_o^2 - \omega^2} + 0 \right) \qquad 2.35$$

Substituting into the expression for μ_c gives: $\mu_c \tilde{=} (\mu' + j\mu'')\left(1 - \frac{k^2}{\mu^2}\right)$

Since latching devices are being considered in this thesis, set $\omega_o = 0$ since $H_o = 0$. Thus:

$$\mu_c \tilde{=} \left(1 - j \frac{\alpha \omega_m}{\omega}\right)\left(1 - \frac{\omega_m^2}{\omega^2}\right)$$

$$\tilde{=} \left[1 - \frac{\omega_m^2}{\omega^2}\right] - j \frac{\alpha \omega_m}{\omega}\left[1 - \frac{\omega_m^2}{\omega^2}\right] \qquad 2.36$$

$$\equiv \mu_c' - j\mu_c''$$

If the propagation constant in a non magnetic, but otherwise equivalent, medium is said to be β_o, then in the magnetic medium the propagation constant will be $\beta_o(\mu_c)^{1/2}$.

In the complex plane μ_c is as is shown in Figure 2.4. In phasor notation:

$$\mu_c = \left[(\mu_c')^2 + (\mu_c'')^2\right]^{1/2} \quad \tan^{-1}\left(\frac{\mu_c''}{\mu_c'}\right)$$

Taking the roots of μ_c gives two solutions as shown in Figure 2.5. A travelling wave in the +z direction varies as $e^{-j\beta z}$, thus the two solutions will be:

$$(1) \quad (\mu_c)^{1/2} = \left[(\mu_c')^2 + (\mu_c'')^2\right]^{1/2} \left[\cos(1/2\theta) + j \sin(1/2\theta)\right]$$

$$(2) \quad (\mu_c)^{1/2} = \left[(\mu_c')^2 + (\mu_c'')^2\right]^{1/2} \left[-\cos(1/2\theta) - j \sin(1/2\theta)\right]$$

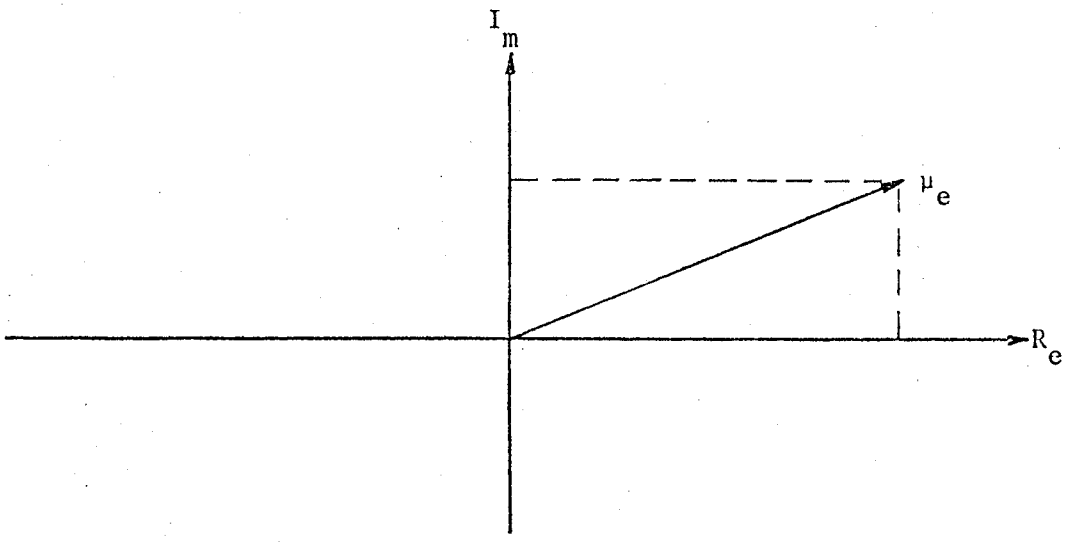

Figure 2.4: μ_e in complex plane.

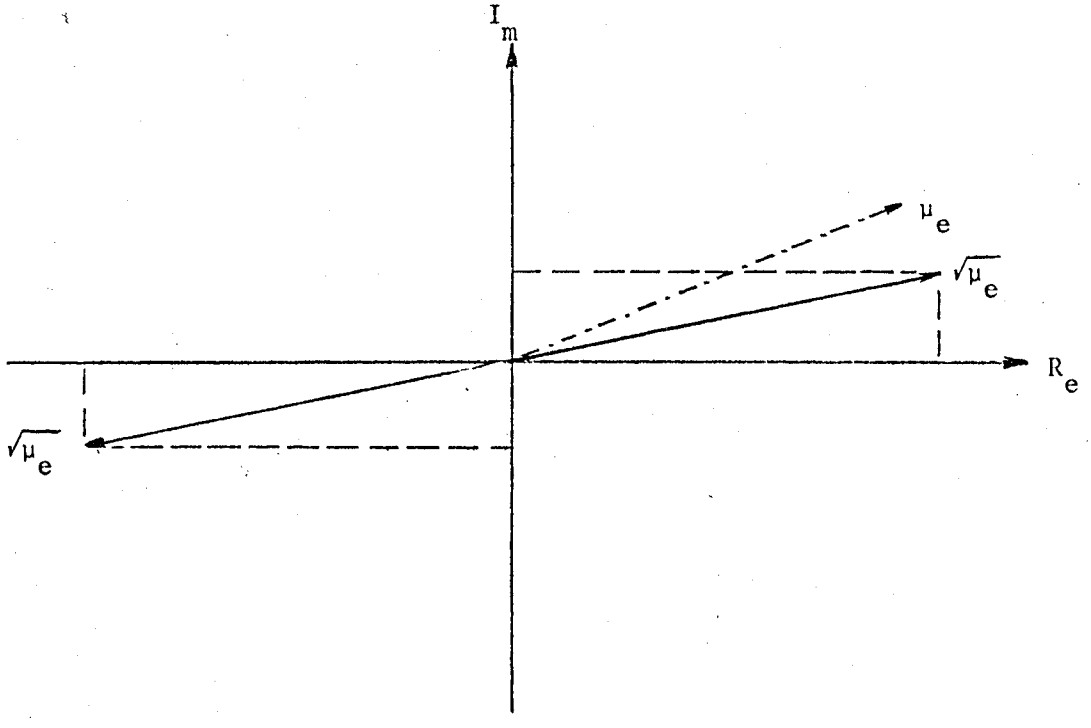

Figure 2.5: $\sqrt{\mu_e}$ in complex plane showing two solutions.

When these solutions are substituted into $e^{-j\beta z}$ where $\beta = \beta_o(\mu_e)^{1/2}$, it is easily seen that the first solution is valid and the second is extraneous since gain through a passive device is not possible. Also since $\mu_e'' << \mu_e'$ then:

$$(\mu_e)^{1/2} \simeq (\mu_e')^{1/2}[\cos(1/2\theta) + j \sin(1/2\theta)] \qquad 2.37a$$

where $\theta = \tan^{-1}\left(\frac{\mu_e''}{\mu_e'}\right)$ 2.37b

Thus the propagation expression is:

$$e^{-j\beta_o(\mu_e')^{\frac{1}{2}}\cos(1/2\theta)z}\ e^{-\beta_o(\mu_e')^{\frac{1}{2}}\sin 1/2\theta} \qquad 2.38$$

The attenuation may be calculated from $e^{-\beta_o(\mu_e')^{\frac{1}{2}}\sin(\frac{1}{2}\theta)z}$ by substituting $\beta_o(\mu_e')^{1/2}z$ equal to the electrical phase length of the device.

2.8 Latching Ferrite Model:

All design equations have been obtained and it remains only to explain the phenomenon of latching ferrites and to derive the classical equations that model this activity. These concepts are not discussed in much of the literature. The best explanation that the author has found is in Reference [3]. In Reference [4], the authors state: "In an unsaturated ferrite, domain resonances exist over the frequency range:

$$\gamma H_{anis} < \omega < \omega_m$$

where H_{anis} is the effective anisotropy field in the material and

$$\omega_m = \gamma(4\pi M_s)."$$

This next section explains why the above statement is valid.

In an infinite saturated ferrite medium, the flux may be represented

by the following equation:

$$B = \mu_o (H_o + H_{int}) \qquad 2.39$$

where H_o is the externally applied field and H_{int} is the internal field resulting from molecular field exchanges. This is shown graphically in Figure 2.6. H_{int} is a constant for a given temperature and is determined by the material, while H_o may be varied by external circuitry. Since $\mu_o=1$ in cgs units and assuming nothing will disturb the system (i.e. $T=0^oK$) then as H_o goes to zero from some large positive value, a state will be obtained where $B = 4\pi Ms = \mu_o H_{int}$

If H goes negative and the system is still not disturbed, the plot would continue in a linear fashion to

$$B = \mu_o H = 0$$

If H_o goes more negative, then H_{int} will change sign creating a single saturated domain magnetized opposite to the initial state as shown in Figure 2.7. This condition is equivalent to the original system but is really a different system since H_{int} is not the same in each case. i.e. $B = \mu_o H$ has a discontinuity at $H = 0$. At temperatures above absolute zero, thermal agitation tends to reduce the alignment action of H which manifests itself in the formation of many saturated domains that are not exactly aligned in the same direction as H_o is applied. If H_o is made large enough, a single domain will result where $B = 4\pi M_s$ but note that $4\pi M_s$ is a decreasing function of temperature. Summing the resultant magnetic domain dipoles will give some B_r which is less than $4\pi M_s$. Inside the domains, however, the fields remain. $H_{int} = 4\pi M_s$

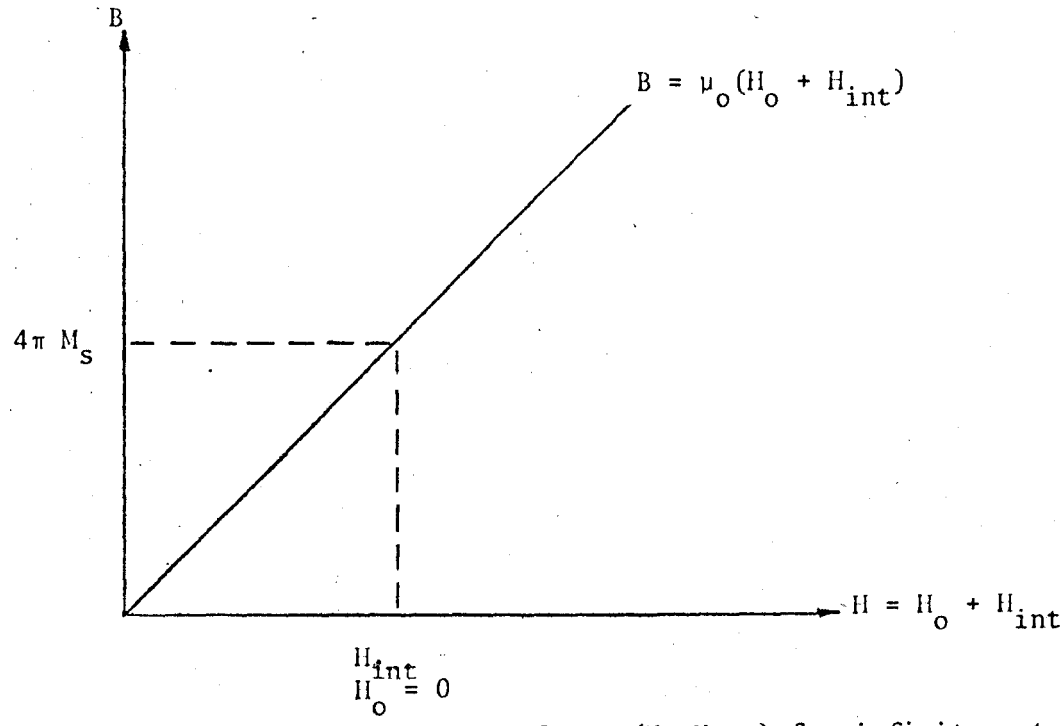

Figure 2.6: Graphical depiction of $B=\mu_o(H_o+H_{int})$ for infinite saturated ferrite at $T = 0^oK$

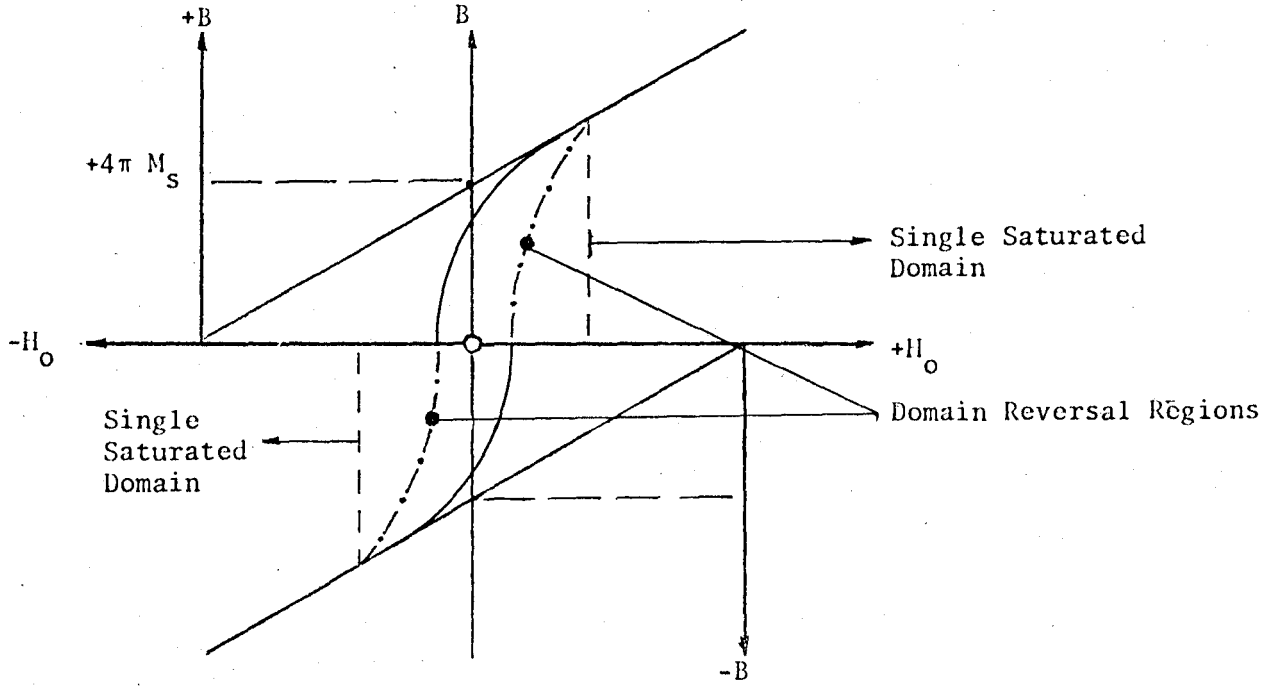

Figure 2.7: Graphical explanation of two magnetized state asymptotes and hysteresis.

plus $$H_o = \frac{B_o}{\mu_o} \qquad 2.40$$

where B_o is the flux due to H_o alone. For an isolated magnetic dipole, it is known the resonant frequency is given by

$$f_r = |\gamma| H_o \qquad 2.41$$

where f_r is the resonant frequency

$|\gamma| = 2.8$ MHz/Oe

H_o is the field applied to the dipole

Thus in the domains that remain aligned to H_o:

$$f_r = |\gamma| (H_o + H_{int}) \qquad 2.42$$
$$= |\gamma| 4\pi M_s \text{ for } H_o = 0$$

Considering each domain as a magnetic dipole of larger magnitude than the elementary molecular dipoles that make up the domain, then these domain dipoles are in a resultant field less than $4\pi M_s$ because of the misalignment of the domains. Calling this effective field that the domains experience as H_{int}^{d}, then the resonant frequency for the domain dipoles is given by:

$$f_r^d = \gamma H_{int}^{d} < f_r \qquad 2.43$$

This theory may be applied to larger domains made up of smaller domains and resulting resonance lines that are successively lower in frequency than the previous lines obtained. The lower limit to these resonant frequencies is given by γH_{anis} which is B_r, i.e. the smallest field experienced by any dipole will be that of the retained magnetism in the remanent state. This γH_{anis} is the ultimate source of remnant magnetization due to molecular

field exchanges as stated in References [3] and [4]. It is easy to see that a complete spectrum of resonance lines would exist between $\gamma H_{anis} = |\gamma| B_r$ and $\gamma H_{int} = |\gamma| 4\pi M_s$ for the remanent state (where $H_o = 0$) thus explaining the quotation from Reference [4] given at the beginning of this section. This region of resonance lines is often referred to as low field losses by many authors. Because the lower end of this spectrum ($\gamma B_r = \gamma H_{anis}$) is not stable due to the physical condition of the ferrite, (for example, hair line cracks would greatly reduce B_r), it is necessary to operate latching devices above $f = |\gamma| 4\pi M_s$. Thus only this area was investigated in this thesis.

Chapter III

Design of Phasers

3.1 General:

In this chapter the designs of two different planar digital latching ferrite phasers will be presented. Where pertinent, the reasons will be given for particular geometries, etc. As in all designs, the actual needs of the user will determine the starting point of the design process. For this reason, the phaser will be assumed and then analyzed following the convention of established authors.

3.2 Transmission Line Structure:

Planar transmission line structures have proved to be very competitive costwise and designwise over conventional wave guide systems. The advantage of these planar structures is well documented elsewhere (Reference [4]) so it remains to select the type of planar transmission line. The two most popular planar structures are microstrip and stripline with microstrip used more often because of its production simplicity. Stripline is not much more costly than microstrip but its use must be justified for any commercial application.

The first consideration is that CRC specifies that the array module is not to exceed 0.6λ in height which is approximately 7.5 inches. The reason for this requirement is that the structure is required to disturb as little as possible the aerodynamics of the aircraft. Thus it is essential

to minimize the size of the total system.

Obviously, the first step in minimizing the size of the structure is to use a high dielectric constant substrate since

$$\lambda_d \simeq \frac{\lambda_o}{\sqrt{\epsilon_{eff}}}$$

where λ_d is the wave length in the dielectric

λ_o is the wave length in free space

and $\epsilon_{eff} = (1-q) + q\,\epsilon_r$

where q is the substrate filling factor. In a microstrip structure the filling factor is approximately 0.6 while for a stripline structure q=1. For example if $\epsilon_r = 10$ then for microstrip $\epsilon_{eff} \simeq 6.4$ while for stripline $\epsilon_r = 10$.

Since the stripline structure confines all the r.f. energy to high dielectric constant regions and microstrip does not, a greater number of wavelengths will be obtained for a given length of line in the stripline structure than in the microstip.

For the Trans Tech. G-400 material used in this thesis where $\epsilon_r = 14$, the ratio of λ_d's for the two types of structure is:

$$\frac{\lambda(\text{micro strip})}{\lambda(\text{strip line})} \simeq 1.6$$

Thus it is seen that significantly shorter lengths of line are needed in the stripline structure.

Another controlling factor on the size of the structure is how close two lines may be placed together without any appreciable coupling.

In most planar phasers, the transmission line is meandered so that a long length of line is confined in a small area. This results in adjacent lines having a certain amount of coupling proportional to the ratio of line separation over substrate thickness. In Reference [4], the authors suggest 5 substrate thicknesses as the minimum separation between lines to prevent significant coupling for the microstrip structure that they describe. In a strip line configuration, the electric flux density is primarily confined directly above and below the centre conductor if it is relatively wide. Thus a separation of 2 substrate thicknesses is sufficient to keep coupling better than 40 dB down (Reference [5] page 129). Because of this, the stripline device allows approximately twice as much line to be confined in the same area as that for a microstrip device. Also, since the fields are completely confined in a stripline structure, there is no problem of coupling between modules in the multi-element phased array system.

For the single aperture device there is also the necessity of having the transmission line imbedded in ferrite material so that transverse remanent magnetization can occur. This will become apparent in the section describing that device.

3.3 Characteristic Impedance:

There are various charts and techniques relating stripline widths, substrate thicknesses and dielectric constants such as in Reference [5]. These graphs give the ratio of width w over b, the ground plane spacing vs. $z_o\sqrt{\varepsilon_r}$ where z_o is the characteristic impedance desired and ε_r is the

relative dielectric constant. Since the applied $\overline{H}_o$ field is zero for a latching device, it may be shown that:

$$\mu_r \tilde{=} 1 - \left(\frac{\omega_m}{\omega}\right)^2 \qquad 3.1$$

for longitudinal magnetization along a toroidal path. For transverse magnetization along a toroidal path, $\mu_r \tilde{-} 1$. (The direction of magnetization is in reference to the direction of the transmission line i.e. the direction of propagation).

As stated in the Chapter II on theory, the mean of the two state impedances should be equal to the impedance of the external connecting circuitry. Thus using Reference [5] it is possible to obtain W/b for $z_o\sqrt{\epsilon_r/\mu_r}$ where ϵ_r is the substrate dielectric constant and $\mu_r \tilde{-} 1 - \frac{1}{2}\left(\frac{\omega_m}{\omega}\right)^2$ 3.2

This stripline width will offer equal power reflection for the two states. Generally speaking $\omega_m/\omega \tilde{-} 0.82 \tilde{-} 0.9^2$. This value will offer a reflection that is approximately 25 dB below the incident signal. Since there is an "in" and an "out" port two reflections occur, thus the reflection is 22 dB below the incident power level.

3.4 Transmission Losses:

Generally, a device will be located in a region where magnetic transmission losses will be very small. To calculate these losses, the 3dB line width as found on the specification sheet for a given material (Appendix I) and the frequency at which the line width is specified are substituted into equation 2.31 to obtain the damping factor α. Substituting

the values for Trans Tech G400 material found in Appendix I the damping factor is:

$$\alpha' = \frac{\gamma \, \Delta H}{2 \, f_s}$$

$$= \frac{-2.8 \text{ MHz/Oe} \times 40 \text{ Oe}}{9.2 \text{ GHz}}$$

$$\simeq -12.2 \times 10^{-3}$$

Next the magnetization resonant frequency is obtained:

$$\omega_m = +2\pi \left[|\gamma| 4\pi M_s \right]$$

$$= +2\pi \left[2.8 \text{ MHz/Oe} \times 400 \text{ Oe} \right]$$

$$= +2\pi \left[1.12 \times 10^9 \right] \text{ rad/sec}$$

The frequency of interest in the case of CRC's AEROSAT system is 1.6 GHz thus $\omega = 2\pi \times 1.6 \times 10^9$ rad/sec

Substituting the values for α, ω_m and ω into 2.36:

$$\mu_e = \left[1 - \left(\frac{\omega_m}{\omega} \right)^2 \right] + j \, \alpha \left(\frac{\omega_m}{\omega} \right) \left[1 - \left(\frac{\omega_m}{\omega} \right)^2 \right]$$

$$\simeq \left[1 - (0.7)^2 \right] + j \, (1.22 \times 10^{-2})(0.7)\left[1-(0.7)^2 \right]$$

$$\simeq 0.51 + j \, (4.36 \times 10^{-3})$$

Thus $\mu_e' \simeq 0.51$

$\mu_e'' \simeq +4.36 \times 10^{-3}$

Substituting these values into 2.37b to obtain the angle of the magnetic loss tangent:

$$\theta = \tan^{-1}\left[\frac{\mu_e''}{\mu_e'} \right]$$

$$= \tan^{-1}\left[+ \frac{4.36 \times 10^{-3}}{0.51} \right]$$

$$\simeq +8.5 \times 10^{-3} \text{ radians}$$

Substituting into 2.37 gives:

$$\sqrt{\mu_e} \simeq \sqrt{\mu_e'}\,[\cos 1/20 + j \sin 1/20]$$

$$\simeq (0.714)[(1.00) + j(4.34 \times 10^{-3})]$$

$$\simeq 0.714 + j3.07 \times 10^{-3}$$

Substituting the imaginary part of $\sqrt{\mu_e}$ into 2.38, the loss may be obtained from:

$$e^{-\beta_o \sqrt{\mu_e'} \sin(1/20)L}$$

$$\simeq e^{-\beta_o (0.003)L}$$

Taking $L = \lambda$ gives the loss per wavelength:

$$e^{-2\pi(0.003)}$$

$$\simeq e^{-0.0188}$$

which is approximately 0.16 dB per wave length. Loss tangents for dielectric losses for materials of interest are of the order of 0.0002, thus are of little concern.

3.5 Double Aperture Phaser:

In Reference [4], a microstrip reciprocal double aperture ferrite phaser is described. In this section, the design of a stripline equivalent to the above mentioned phaser is presented. Some reasons for using stripline rather than micro-strip techniques have already been stated in Section 3.2. Also since, the single aperture device described in Section 3.6 must be of the stripline type so that transverse magnetization may occur, the double aperture device was similarly constructed in stripline for comparative reasons.

The geometry of this device showing the two magnetized states is shown in Figures 3.1a and 3.1b. Since only along a line between each pair of holes would the magnetization be parallel to or at right angles to the transmission line, it is necessary to perform the following lengthy but relatively simple mathematical calculation to derive the actual differential phase shift through the device. A picture of this device is shown at the beginning of the thesis.

In Figure 3.1a, the magnetization is more parallel than perpendicular to the meandered line section. The dotted input and output lines experience the same effective permeability in either state. The magnetization is circular in nature about each hole s and it is assumed that all the meandered line is in a switched zone. It is apparent from the diagram that line section fe is not truly in a switched zone, however, field inhomogeneities would make this region essentially a switched region

Recall that $\mu_{\perp} \tilde{=} 1$

$$\mu_{\parallel} \tilde{=} 1 - \left(\frac{\omega_m}{\omega}\right)^2$$

Thus $$\mu \tilde{=} 1 - \left(\frac{\omega_m}{\omega}\right)^2 \cos\theta$$

where $\cos\theta = \dfrac{x}{\sqrt{x^2+y^2}}$

It is apparent from Figures 3.1a and 3.1b that: the differential phase for the sum of line sections: [bc + dc + fg + hj] will cancel the differential phase of line section kj. It is also easy to see that the symmetry about the line joining the hole pairs will simplify the integrations as below.

Using a Taylor series first order approximation gives:

$$\sqrt{\mu} \tilde{-} 1 - \frac{1}{2}\left(\frac{\omega_m}{\omega}\right)^2 \cos\theta$$

$$\tilde{-} 1 - \frac{1}{2}\left(\frac{\omega_m}{\omega}\right)^2 \left(\frac{x}{\sqrt{x^2+y^2}}\right)$$

Thus the phase length of the meandered line in this state is approximately:

$$\phi_{11} \tilde{-} 2\int_o^b \beta_o \left[1 - \frac{1}{2}\left(\frac{\omega_m}{\omega}\right)^2 \left(\frac{x}{\sqrt{x_1^2+y^2}}\right)\right]dy$$

$$+ 4\int_o^c \beta_o \left[1 - \frac{1}{2}\left(\frac{\omega_m}{\omega}\right)^2 \left(\frac{x}{\sqrt{x_2^2+y^2}}\right)\right]dy$$

$$+2\int_o^f \beta_o \left[1 - \frac{1}{2}\left(\frac{\omega_m}{\omega}\right)^2 \left(\frac{x_3}{\sqrt{x_3^2+y^2}}\right)\right]dy$$

$$+ \left[\phi_{11}(k_j) + \phi_{\perp}\right](bc + de + fg + hj) = \phi_c$$

$$\phi_{11} \tilde{-} 8\,A\beta_o + \phi_c$$

$$-\beta_o\left(\frac{\omega_m}{\omega}\right)^2 (X_1)\left[\log\left(A + \sqrt{A^2+X_1^2}\right) - \log(X_1)\right]$$

$$-2\beta_o\left(\frac{\omega_m}{\omega}\right)^2 (X_2)\left[\log\left(A + \sqrt{A^2+X_2^2}\right) - \log(X_2)\right]$$

$$-\beta_o\left(\frac{\omega_m}{\omega}\right)^2 (X_3)\left[\log\left(A + \sqrt{A^2+X_3^2}\right) - \log(X_3)\right] \qquad 3.3$$

In Figure 3.1b, the magnetization is more perpendicular than parallel to the meandered line section. The dotted input and output lines experience the same effective permeability in either state shown in Figure 3.1. Again, the magnetization of the substrate is circular about each hole T and as before it is assumed that all of the meandered line is in a switched region.

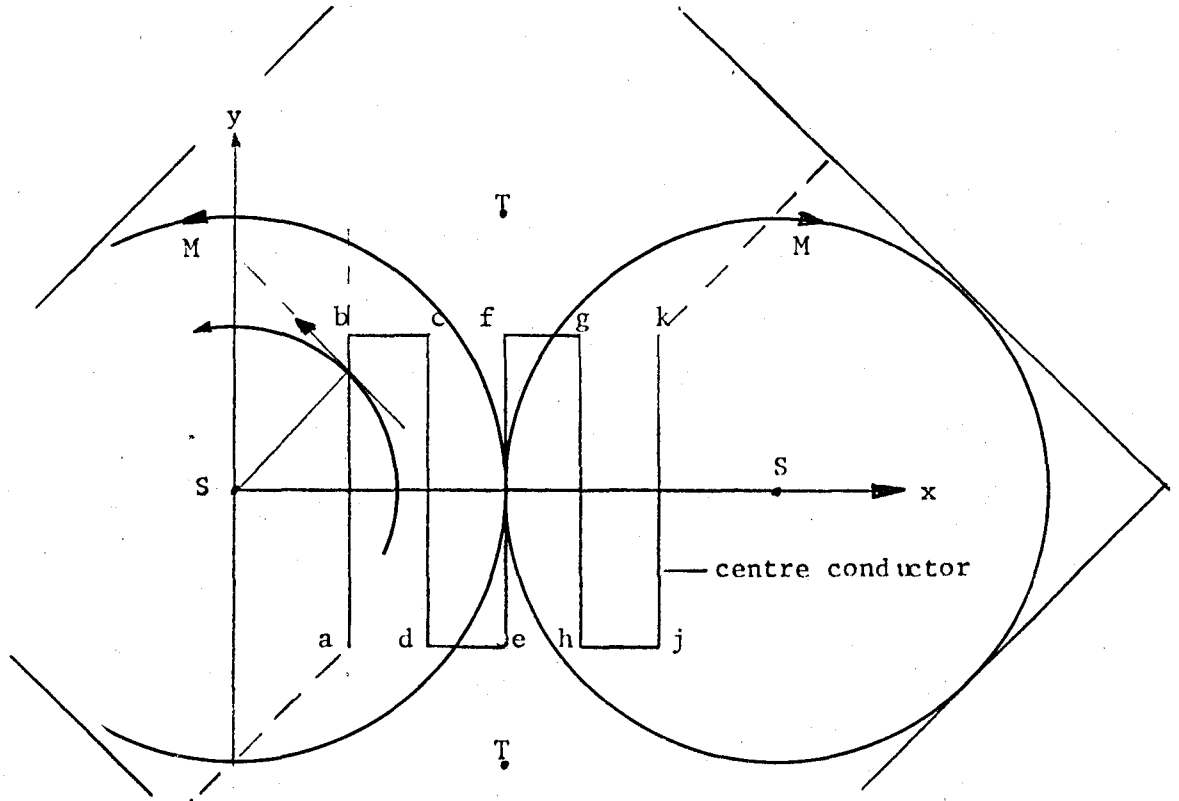

Figure 3.1a: Double aperture parallel magnetization (2x 2x .025 in.plate)

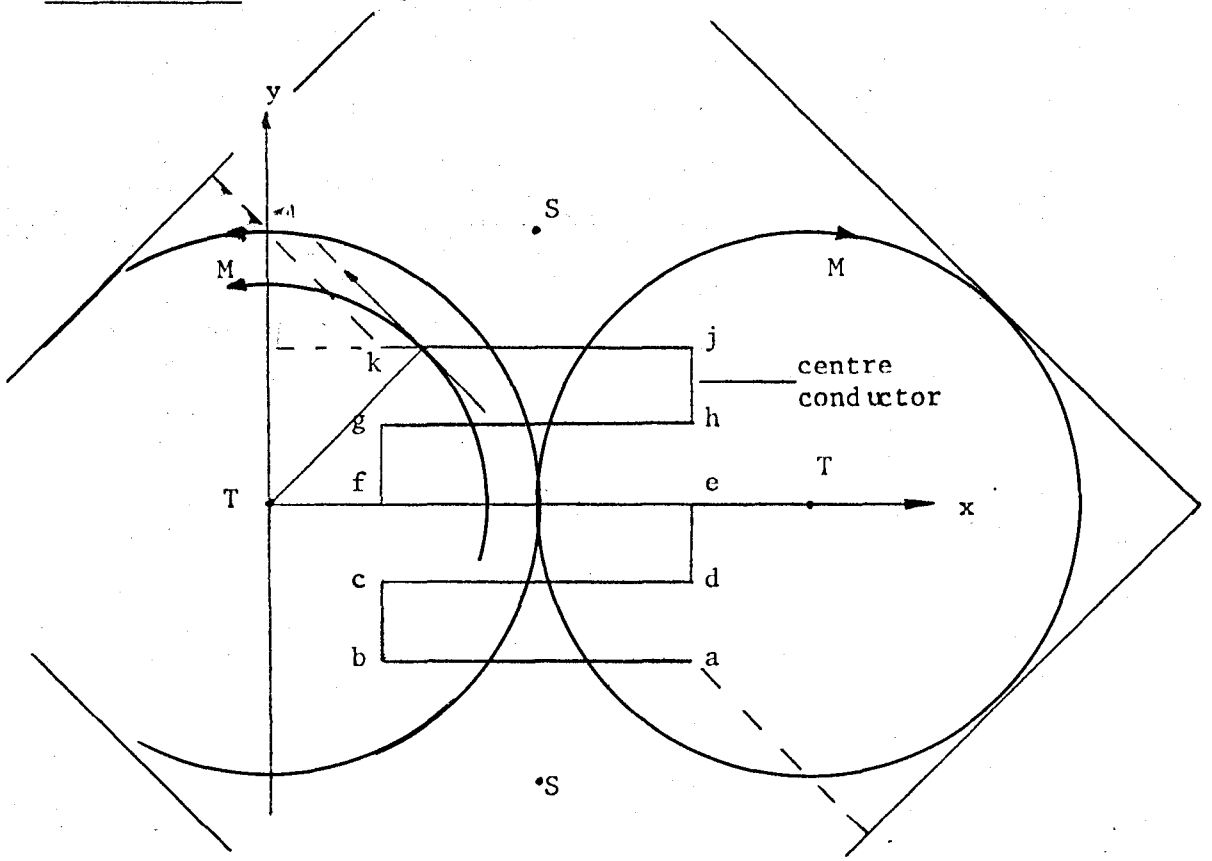

Figure 3.1b: Double aperture perpendicular magnetization
(2x 2x .025 in. ferrite plate

As stated previously line section fe experiences completely transverse magnetization in the state depicted in Figure 3.1b. In Figure 3.1a, portions of the line are in an unmagnetized region. However, since the demagnetizing field normal to the plate plane is almost unity, the magnetic domains under fe must resolve along the x and y axes, thus the permeability will be approximately $\mu_{eff} \tilde{-} 1 - \frac{1}{2}\left(\frac{\omega_m}{\omega}\right)^2$. Since in this calculation only first order approximations are being considered, the above discrepancy is not significant. Recall again:

$$\sqrt{\mu} \tilde{-} 1 - \frac{1}{2}\left(\frac{\omega_m}{\omega}\right)^2 \cos\theta$$

where $\cos\theta = \frac{y}{\sqrt{y^2+x^2}}$ in this case

Thus $\sqrt{\mu} \tilde{-} 1 - \frac{1}{2}\left(\frac{\omega_m}{\omega}\right)^2 \frac{y}{\sqrt{y^2+x^2}}$

Then

$$\phi_{\perp} = 2\int_A^R \beta_o\left[1 - \frac{1}{2}\left(\frac{\omega_m}{\omega}\right)^2 \left(\frac{y_2}{\sqrt{y_2^2+x^2}}\right)\right]dx$$

$$+ 4\int_A^R \beta_o\left[1 - \frac{1}{2}\left(\frac{\omega_m}{\omega}\right)^2 \left(\frac{y_1}{\sqrt{y_1^2+x^2}}\right)\right]dx$$

$$+ 2A\beta_o + \left[\phi_{\perp}(b_j) + \phi_{11}(bc+de+fg+hj) = \phi_c\right]$$

$$\phi_{\perp} = 3A\beta_o + \phi_c$$

$$-\beta_o\left(\frac{\omega_m}{\omega}\right)^2 (Y_2)\left[\log\left(R + \sqrt{R^2+Y_2^2}\right) - \log\left(A + \sqrt{A^2+Y_2^2}\right)\right]$$

$$-2\beta_o\left(\frac{\omega_m}{\omega}\right)^2 (Y_1)\left[\log\left(R + \sqrt{R^2+Y_1^2}\right) - \log\left(A + \sqrt{A^2+Y_1^2}\right)\right] \qquad 3.4$$

Now that expressions for the electrical length have been obtained for each state, it is possible to obtain the differential phase shift of the device by taking the difference between equations 3.3 and 3.4

Thus $\Delta\phi = \phi_{\perp} - \phi_{11}$

$$= \beta_o \left(\frac{\omega_m}{\omega}\right)^2 \left[(X_1)\{\log(A + \sqrt{A^2+X_1^2}) - \log(X_1)\}\right.$$

$$+ 2(X_2)\{\log(A + \sqrt{A^2+X_2^2}) - \log(X_2)\}$$

$$+ (X_3)\{\log(A + \sqrt{A^2+X_3^2}) - \log(X_3)\}$$

$$- (Y_2)\{\log(R + \sqrt{R^2+Y_2^2} - \log(A + \sqrt{A^2+Y_2^2})\}$$

$$\left. - 2(Y_1)\{\log(R + \sqrt{R^2+Y_1^2} - \log(A + \sqrt{A^2+Y_1^2})\}\right] \qquad 3.5$$

By substituting the appropriate numbers into equation 3.5 it is possible to obtain the differential phase shift for the device. This will be done in the next chapter so as to compare with experimental data. Of course, if other than 5 meandered line sections occur, or if the meandered line region is not a square area, then equation 3.5 and the derivation producing this result will have to be changed appropriately.

3.6 Single Aperture Phaser:

The single aperture phaser described in this section is an attempt to make more efficient use of the ferrite material than is made in the double aperture phaser of section 3.5. The principles of design are valid. However, because of certain problems with the available technology, it was

not possible to verify without question the validity of this design experimentally. Initially the design will be described and then the problems due to the fabrication process will be explained showing why the device does not work as well as the theory predicts.

The geometry of the centre conductor is shown in Figure 3.2. When a current pulse is passed normal to the plane of the structure through the centre hole, a circular magnetization will occur in the substrate that is parallel to the majority of the meandered line sections.

In Figure 3.3 is shown how transverse magnetization of the substrate occurs. By sending current pulse down the r.f. centre conductor, the ferrite material around the centre conductor should become magnetized in the directions shown in Figure 3.3 which is essentially parallel to the h_{rf} of the propagating r.f. signal. Separation between adjacent r.f. conductors must be a minimum of the ground plane spacing so that complete magnetization of the material above and below the r.f. centre conductor may occur. This spacing is sufficient to keep coupling at least 40 db down as stated in section 3.5. In this magnetic remanent state, there is little interaction between, the h field of the r.f. wave and the substrate, thus $\mu \tilde{-} 1$. Also since the r.f. field oscillates so rapidly at any given point, ferrite remanent magnetization processes (domain wall relations and reversals) do not respond to the h_{rf} as these processes are inherantly slow.

Thus the two magnetic states offer an effective permeability of:

$$\mu_{||} \tilde{-} 1 - \left(\frac{\omega_m}{\omega}\right)^2$$

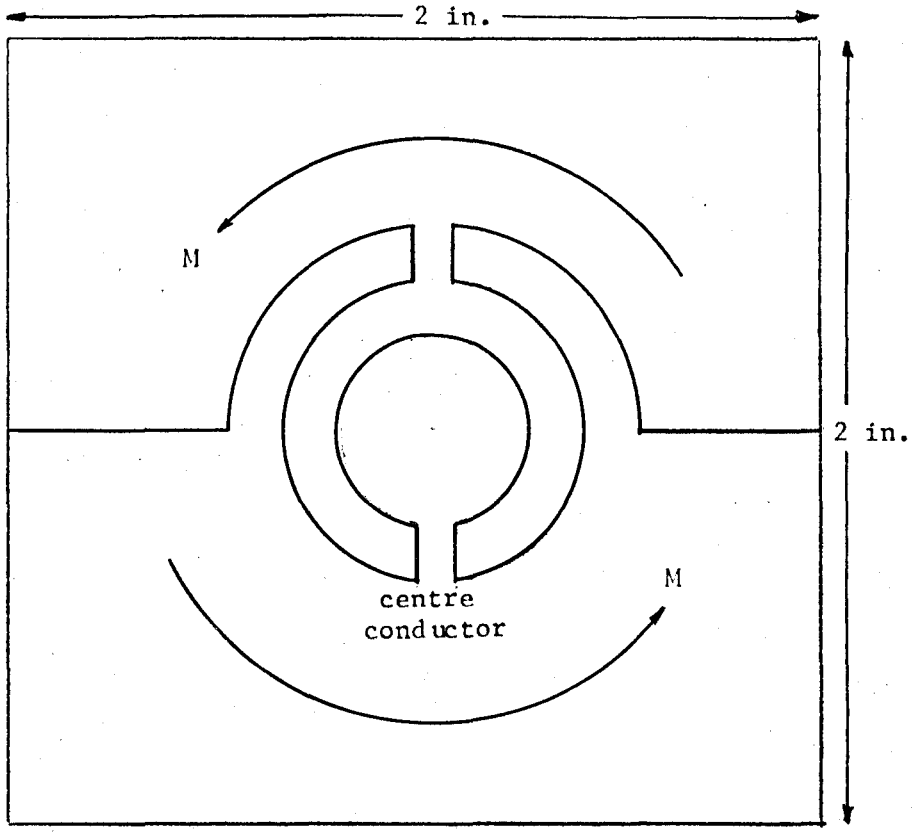

Figure 3.2: Geometry of center conductor for single aperture device showing parallel magnetization poles

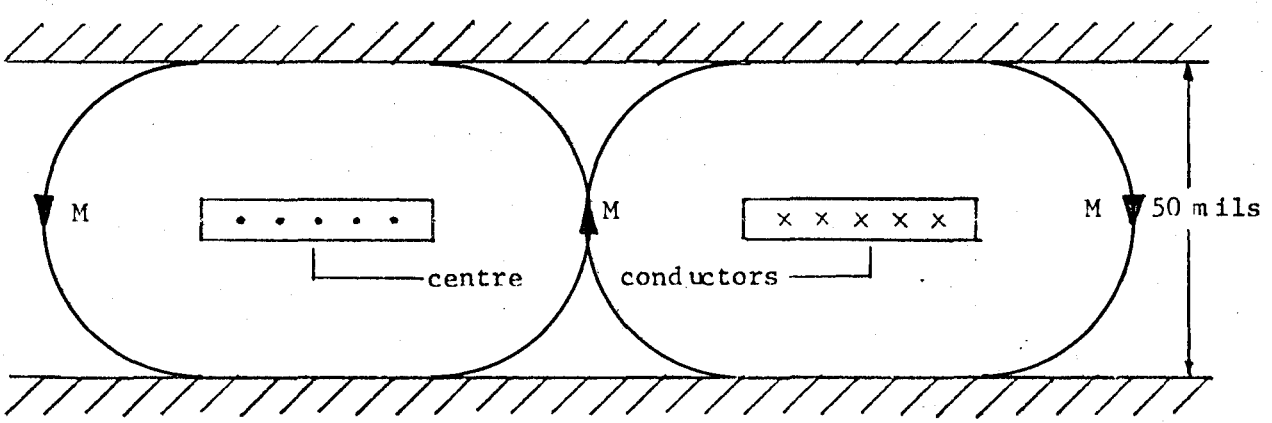

Fig. 3.3: Transverse magnetization of ferrite material for single aperture device.

and $$\mu_{\perp} \simeq 1$$

By adding up the lengths of the circular portions of the r.f. centre conductor and as before taking a first order Taylor approximation for $\sqrt{\mu}$ the differential phase shift is found to be:

$$\Delta\phi \simeq \frac{1}{2} \beta_o \left(\frac{\omega_m}{\omega} \right)^2 L$$

where L is the total length of meandered circular centre conductor in the device. Obviously, the design of the above device is much simpler than that of the double aperture phaser. It also offers the advantage that essentially all of the substrate surface may be used (excepting the corners) whereas with the double aperture device, only a centre square area approximately equal to 1/9 of the surface area may be used. The reason for this is that, the toroidal path about each hole must be such that a equal return path for the flux must exist on the outer portions of the substrate. Otherwise the centre region will not magnetize completely. This is so since the flux density in the material is essentially a constant on the macroscopic scale.

The second design in theory makes it possible to obtain a much larger phase shift for a given area than is possible with the design of Section 3.6. However, to produce this device would be much more costly than the double aperture phaser since the design is based on the center conductor being imbedded in ferrite material. This is not practical in any production run and it is also very difficult to produce under laboratory conditions. The technique used to produce this device for experimental testing involved two substrate plates with the centre conductor

being produced on one plate using standard photo lithography techniques and then "sandwiching" the two substrates between two aluminum ground planes. This left an air gap between the two plates which is the origin of the discrepancy between experiment and theory as presented in the next chapters. A further discussion of this topic will be presented in Chapter V.

Chapter IV

Experimental Results:

4.1 General:

In this thesis, the experimental results of a double aperture and a single aperture reciprocal ferrite latching phase shifter are presented. Approximately fifty different devices were built in the investigation of this thesis which culminated in this presentation of these two devices.

Copper or aluminum laminated ferrite plates were not available from the manufacturer and since thick film deposition facilities were not available at McMaster, the centre conductor was produced by glueing a 2 mil thick sheet of copper foil to one plate. Then the circuit was produced by standard photolithographic techniques. However for the material G-400 with a dielectric constant of $\varepsilon_r = 14.1$ and a substrate thickness of 0.025 inches, a 50 Ω line would only be 0.005 inches wide. The copper deposition technique left small surface irregularities etc. making it impossible to etch a 5 mil line. Thus it was arbitrarily decided to make the line 25 mils wide and obtain experimental results for the phase shift only. Insertion losses were of the order of about 2 dB from 1.1 to 2.0 GHz. Because of this high insertion loss it was not possible to determine the magnetic losses in each of the two states.

A further discussion of the problem encountered in fabricating these devices is presented in Appendix II.

4.2 Double Aperture Phaser:

The double aperture phaser described in this thesis had the configuration shown in Figure 3.1. The dimensions are given in Table 4.1. The substrate thickness was 0.025 mils, thus ground plane spacing was approximately 0.55 inches. The copper centre conductor plus the adhesive account for the extra 5 mils.

Table 4.1

Double Aperture Phaser Dimensions

A = 0.4 inches	R = 0.7 inches
X_1 = 0.3 inches	Y_1 = 0.2 inches
X_2 = 0.5 inches	Y_2 = 0.4 inches
X_3 = 0.7 inches	

Substituting the values of Table 4.1 into equation 3.5 gives:

$$\Delta\phi = \beta_o \left(\frac{\omega_m}{\omega}\right)^2 \Big[(0.3)\{\log(0.4 + \sqrt{(0.4)^2+(0.3)^2} - \log(0.3)\}$$

$$+ 2(0.5)\{\log(0.4 + \sqrt{(0.4)^2+(0.5)^2}) - \log(0.5)\}$$

$$+ (0.7)\{\log(0.9 + \sqrt{(0.4)^2+(0.7)^2} - \log(0.7)\}$$

$$- (0.4)\{\log(0.7+\sqrt{(0.7)^2+(0.4)^2}) - \log(0.4 + \sqrt{(0.4)^2+(0.4)^2})\}$$

$$-2(0.2)\{\log(0.7+\sqrt{(0.7)^2+(0.2)^2}) - \log(0.4 + \sqrt{(0.4)^2+(0.2)^2})\}$$

$$= \beta_o \left(\frac{\omega_m}{\omega}\right)^2 (0.81) \text{ radians} \qquad 4.1$$

where $$\beta_o = \left(\frac{\omega \sqrt{\varepsilon_r} \times 2.54}{3 \times 10^{10}}\right)\left(\frac{\text{radians}}{\text{inch}}\right)$$

$$= 114\ f(\text{GHz}) \text{ degrees/inch.}$$

and $$\omega_m = 2\pi|\gamma|4\pi M_s$$

$$= 2\pi(2.8 \text{ MHz}/O_e) \times 400\ O_e$$

$$= 2\pi(1.12 \times 10^9) \text{ radians/sec.}$$

By substituting the appropriate values into equation 4.1, the theoretical plot of differential phase shift for the saturated device may be obtained as shown in Figure 4.1 by the solid line. The experimental data for the device (Table 4.2) was produced by an HP-8545A network analyser system. The network analyser was patched into a CDC-6400 computer at McMaster in which resided a routine that controlled the measurement taking and processed the data. Each measurement was made 25 times by the system and then the results were averaged giving the phase length versus frequency information in Table 4.2. In Table 4.3 the differential phase is calculated from Table 4.2 and this information is ploted on Figure 4.1. Note that the theoretical data assumes a saturated magnetic state for the substrate.

Table 4.2 Double Aperture Phaser

Frequency in MHz	Transverse Magnetic State S21 Phase (Radians)	Longitudinal Magnetic State S21 Phase (Radians)
1100	-2.83804	-3.14837
1150	-2.88115	2.60242
1200	2.265	1.98354
1250	1.67667	1.36374
1300	1.01952	.735545
1350	.383795	.124856
1400	-.195673	-.412739
1450	-.714719	-.911478
1500	-1.23775	-1.42918
1550	-1.74216	-1.93776
1600	-2.26757	-2.4674
1650	-2.85287	-3.04978
1700	2.86725	2.6803
1750	2.36172	2.19001
1800	1.83315	1.68261
1850	1.35907	1.21013
1900	.862222	.69538

Experimental data of phase length for two magnetic states for double aperture phaser. (S21 is the transmission parameter of the scattering matrix.)

Table 4.3 Double Aperture Phaser

Frequency in Mlz	$\Delta\phi$ (rad)	$\Delta\phi$ (deg)
1100	.31033	17.8
1150	.27873	15.0
1200	.28146	16.1
1250	.31293	17.9
1300	.28396	16.3
1350	.25894	14.8
1400	.21707	12.4
1450	.19676	11.3
1500	.19143	11.0
1550	.19560	11.2
1600	.19983	11.5
1650	.19691	11.3
1700	.18695	10.7
1750	.17171	9.8
1800	.15059	8.6
1850	.14894	8.5
1900	.16684	9.6

Differential phase shift calculated from Table 4.2 for double aperture phaser.

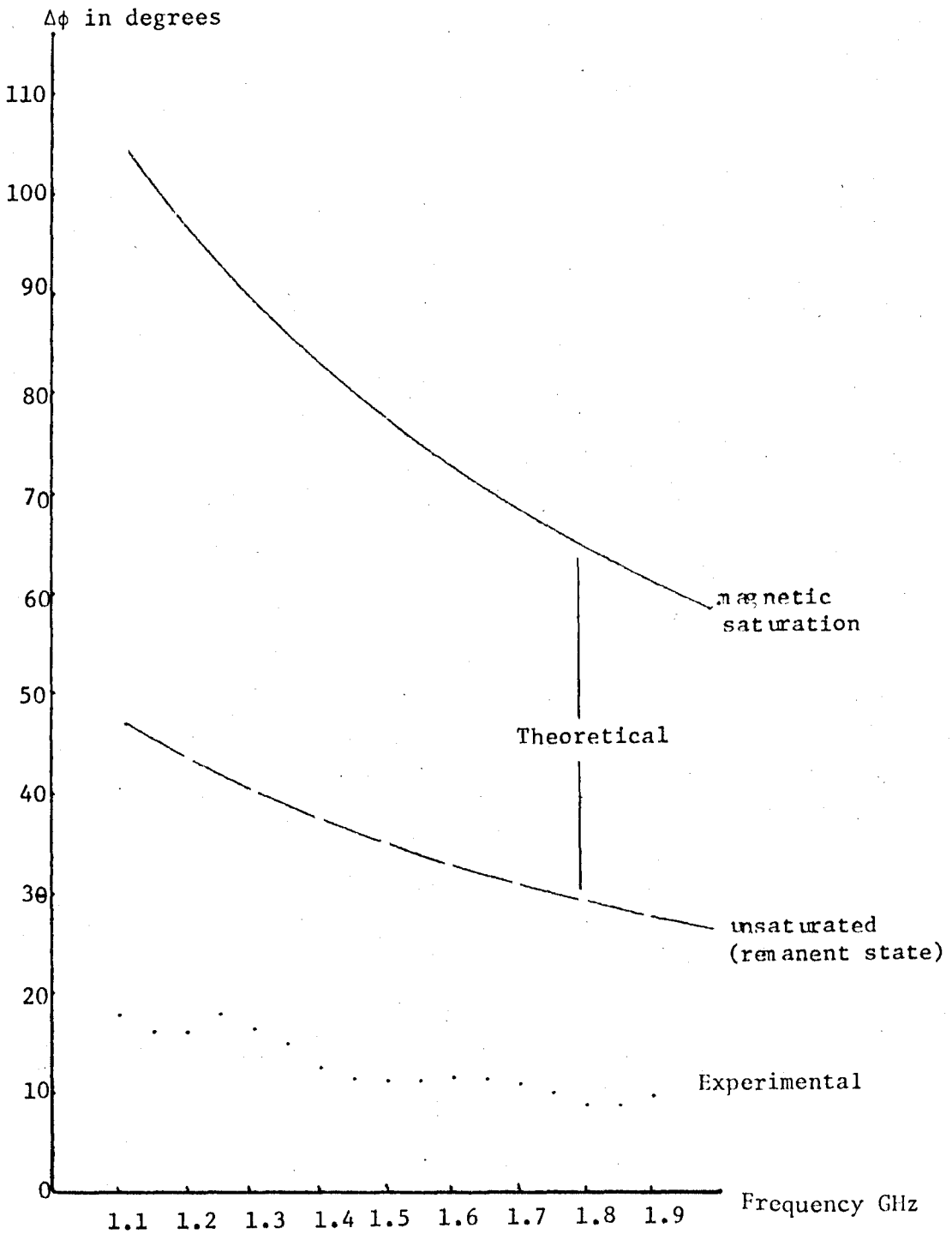

Figure 4.1: Plots of theoretical saturated differential phase shift; corrected for non saturation effects and experimental data for double aperture device.

4.3 Single Aperture Phaser

The single aperture phaser described in this thesis had the configuration shown in Figure 3.2. The dimensions are given in Table 4.4 and as with the double aperture device, the substrate thickness was 0.025 mils giving a ground plane spacing of approximately 55 mils. The material used was the same Trans Tech G-400 material used in the double apperture device. The fabrication process was also the same for both devices. In effect both devices were equivalent with respect to technology; only the designs of the centre conductors and the magnetic remanent states were different for each device.

Table 4.4

Single Aperture Phaser Dimensions

d_1 = 0.475 inches S = 0.100 inches.

d_2 = 0.775 inches

d_3 = 1.075 inches.

Taking equation 3.6, it is possible to obtain L = 5.40 inches from Table 4.4

Thus
$$\Delta\phi \simeq \beta_o \left(\frac{\omega_m}{\omega} \right)^2 L \qquad 3.6$$

where $\beta_o \equiv 114\ f(\text{GHz})$ degrees/inch

$\omega_m = 2\pi\ |\gamma|\ 4\pi\ M_s$

$= 2\pi\ (1.12 \times 10^4)$ radians/inch

and $L = 5.40$ inches

By substituting the above values in to equation 3.6 it is possible to obtain a plot of $\Delta\phi$ versus frequency. This plot is, as before, a first order

approximation to a saturated ferrite device. It would be quite simple to calculate the exact theoretical $\Delta\phi$ but because a first order approximation was necessary for mathematical simplification with the double aperture device, the same was done here. Thus a more valid comparison between the devices may be obtained.

The theoretical plot and the experimental data of Tables 4.5 and 4.6 are plotted in Figure 4.2

Table 4.5 Single Aperture Phaser

Freq (GHz) Frequency	Transverse Magnetic State Phase Angle (Radians) S21 Phase (Radians)	Longitudinal Magnetic State Phase Angle (Radians) S21 Phase (Radians)
1100	1.55592	1.25386
1150	.557097	.293573
1200	-.288274	-.492805
1250	-.980873	-1.15541
1300	-1.6786	-1.87441
1350	-2.45663	-2.67947
1400	3.04168	2.83021
1450	2.30544	2.12813
1500	1.60892	1.42352
1550	.939758	.761169
1600	.262986	7.42732E-03
1650	- .525088	-.691182
1700	-1.20602	-3.02623
1750	-1.83259	-1.94604
1800	-2.45052	-2.56602
1850	-3.13111	3.05331
1900	2.45545	2.3339

Experimental data of phase length for two magnetic states for double aperture phaser. (S21 is the scattering parameter.)

Table 4.6 Single Aperture Phaser

Freq in MHz	$\Delta\phi$(radians)	$\Delta\phi$(degrees)
1100	.30206	17.3
1150	.26352	15.1
1200	.20455	11.7
1250	.17254	9.9
1300	.19581	11.2
1350	.22284	12.8
1400	.21147	12.1
1450	.17731	10.2
1500	.18540	10.6
1550	.17859	10.2
1600	.19556	11.2
1650	.16609	9.5
1700	Wrong	
1750	.11345	6.5
1800	.11550	6.6
1850	.0980	5.6
1900	.12155	7.0

Differential phase shift calculated from Table 4.5 for single aperture phaser.

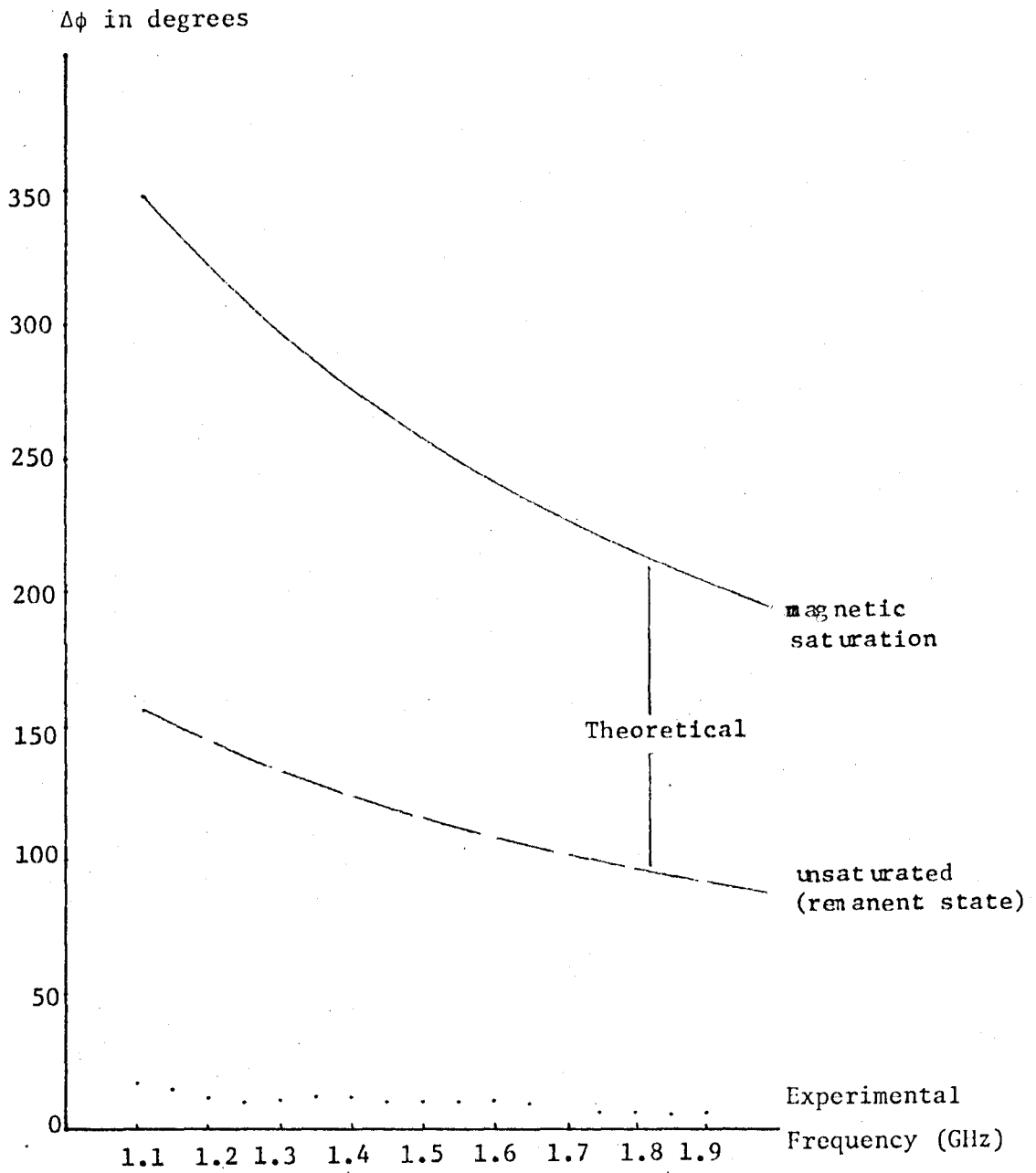

Figure 4.2: Theoretical, corrected theoretical and experimental data for single aperture device.

Chapter V

Conclusions

5.1 General:

At best, the theory of ferrites offers only an order of magnitude feeling for the actual obtainable phase shifts. The first sort of error to be considered is that the ferrite specimens considered in this thesis are not magnetized to saturation as was assumed. Because of the domain structure and the resulting misalignment of the various magnetic dipoles, the two magnetic states are not orthogonal. A good approximation to the actual state is that B_m indicates the actual magnetization that is parallel to the desired direction while $4\pi M_s - B_m$ will resolve mostly to the perpendicular direction. Thus in effect the effect of each state must be multiplied by the ratio of $B_m/4\pi M_s$ so as to correct for the error in the alignment.

Physically this misalignment does not allow as much energy storage in the dipole precessions as would be possible if alignment were exact. Conversly for the none interacting state some energy storage does occur when it is assumed that none occurs. In effect:

$$\mu_{\perp} > 1$$

and

$$\mu_{11} < 1 - \left(\frac{\omega_m}{\omega}\right)^2$$

Taking the ratio of retained magnetism to the saturated magnetism then:

$$\mu_{\perp} \tilde{=} 1 - \left(\frac{4\pi M_s - B_m}{4\pi M_s}\right)\left(\frac{\omega_m}{\omega}\right)^2 \qquad 5.1$$

$$\mu_{11} \tilde{=} 1 - \left(\frac{B_m}{4\pi M_s}\right)\left(\frac{\omega_m}{\omega}\right)^2 \qquad 5.2$$

Thus the differential phase shift would be:

$$\Delta\phi \tilde{=} \beta_o L_e[\sqrt{\mu_{11}} - \sqrt{\mu_{\perp}}] \qquad 5.3$$

where $\beta_o = \omega\sqrt{\mu_o \varepsilon_o \varepsilon_r}$

and L_e is the effective length of switched line in the ferrite environment. Taking a Taylor first order approximation to equation 5.3 gives:

$$\Delta\phi \tilde{=} \beta_o L \left[\frac{2 B_m}{4\pi M_s} - 1\right] \qquad 5.4$$

Thus if all theoretical phase shifts are multiplied by the factor

$$\left[\frac{2 B_m}{4\pi M_s} - 1\right] \qquad 5.5$$

a first order error correction will be made for the fact that the material is not saturated.

5.2 Double Aperture Phaser:

Considering the double aperture device of this thesis then substituting the values for B_n and $4\pi M_s$ for the G-400 material, the correction factor becomes $\frac{2 B_m}{4\pi M_s} - 1 \tilde{=} 0.45$. By multiplying the theoretical curve of figure 4.1 by the factor 0.45, a curve that is closer to the experimental data is obtained. It must be emphasised that this corrected curve shown in Figure 4.1 (dashed line) is only a first order approximation. The deviation

between this plot and data is due to the 2 to 3 mil separation between the centre conductor and the ferrite plate caused by the adhesive. The non monotonic nature of the experimental results which are repeatable has not been explained.

5.3 Single Aperture Phaser:

As with the double aperture device anerror correction factor of 0.45 should multiply the theorectical saturated phase shift of Figure 4.2. This is shown as a dashed line in Figure 4.2. However the experimental data is still substantially below this corrected curve.

The explanation for this was determined to be as a result of the fabrication technique. Since, the phaser was constructed of two plates with the centre conductor sandwiched between the plates, there resulted an air gap of approximately 5 mils. Thus the toroidal path of magnetic flux around the transmission line (Figure 3.2b) has two air gaps in it. These gaps create poles along the surface of the plates adjacent to the conductors and as a result a demagnetizing field is produced. This demagnetizing field tends to reduce the alignment of the desired magnetic state where the magnetic dipoles would be at right angles to the direction of propagation. The actual demagnetizing fields were not calculated for this thesis because of their complexity. However, a qualitative argument may be presented that indicates this is the reason for the lower than expected phase shift. Assuming that the magnetic flux density in the air gap is the same as in a magnetized ferrite toroidal path i.e. for G-400 $B_g \tilde{-}$ 290 Gauss. Then across the air gap the magnetic intensity drop would

be:

$$H_g \times L_g \tilde{-} 3.7 \text{ Gilberts.}$$

where H_g = 290 Oersteds; the field intensity in air for a flux density of 290 Gauss

L_g = 0.005 x 2.54 = 0.0127 cm

The maximum DC magnetic flux path length around the strip line is approximately 0.5 cm. With H_c = 0.69 Oersteds this is equivalent to a field approximately of 0.4 Gilberts required to demagnetize the ferrite toroid without air gaps. Thus the 3.7 Gilbert drop of the air gap indicates a much wider pole distribution than the assumed area and/or a much lower flux density in the ferrite than assumed. Obviously some distribution that gives a lower flux density (i.e. due to a demagnetizing field) and a larger than 0.025 in. wide pole distribution exists in combination to give the observed effect.

To overcome this problem, the ratio of the air gap over the total flux path length must be reduced. Obviously the best result would be to reduce the air gap to zero but this involves fabricating the ferrite material with the conductor in the middle which would be expensive to say the least. Staying with the double plate concept, if a method of depositing 100,000 $\mathring{A}$ (approximately 5 skin depths) of conductor on the ferrite material is available, then the air gap is reduced to 10 microns.

The other thing that may be done is to make the substrate thicker. This has the effect of making the transmission line wider and thus making the path through the ferrite longer.

5.4 Comparison of Two Designs:

In the double aperture device only the centre square region of the plate may be used to produce a phase shift. This is approximately one ninth of the total area of ferrite plate.

In the single aperture device, the whole plate may be used, however, only an average of one fourth approximately of the possible phase shift is obtained using the available construction techniques.

Assuming a separation between adjacent lines of 0.1 inches on a 2x2 inch plate then in a double aperture phaser, the possible effective length of switched line is approximately nine inches. In the single aperture device, the effective length of switched line would be approximately twenty seven inches. Thus there is a ratio of 3:1 in possible line lengths between the two devices. By combining these two figures, it is easy to see that only 3/4 of the possible phase shift obtainable in the double aperture phaser may be obtained in the single aperture device. Thus, unless some technique of greatly reducing the ratio of air gap to flux path length in the devices is obtained, there is no justification for using the single aperture design. Using thick film deposition techniques should make it possible to do this.

APPENDIX 1

Ferrite Specifications

On the following page is given a photocopy of the specification sheet for the ferrite material used in this thesis. These specifications are those provided by Trans Tech, Inc. for the material they designate as G-400 which is an aluminum doped garnet polycrystalline ceramic.

TRANS-TECH, INC.
GARNETS • FERRITES • ALUMINA
DIELECTRICS • CUSTOM R & D

SPECIFICATION BULLETIN 68.

GARNET
BULLETIN NO. 155-67

TYPE G-400
Aluminum doped

CHARACTERISTICS

Saturation Magnetization ($4\pi M_s$) in gauss @ 23°C	400 ±25 gauss
g-effective @ 9.4 GHz	2.01 ±1%
Line Width (ΔH) in oersteds @ −3db and 9.4 GHz	< 45
Line Width (ΔH) in oersteds @ −15db and 9.4 GHz	< 200
Dielectric Constant (ϵ') @ 9.4 GHz	14.1 ±5%
Dielectric Loss Tangent ($\tan\delta$) @ 9.4 GHz	< .0002
Curie Temperature in °C	135
Spin Wave Line Width (ΔH_k) in oersteds @ 9.4 GHz	1.40
Switching Coefficient* (S_w) in oersted • μsec	0.58
Switching Intercept* (H_0) in oersteds	0.79
Initial Permeability (μ_0) @ 1 KHz	41

*10% output voltage measurement

Material Type G-400 is one of a series of aluminum doped yttrium-iron garnets. This series exhibits very narrow resonance line widths and finds primary application in non-resonant devices where extremely low absorption loss is required. Also, the absence of rare earths such as gadolinium makes them the most suitable yttrium type garnets for cryogenic applications. The useful frequency range for type G-400 extends from 0.18 to 1.8 GHz depending on the device geometry demagnetizing factor.

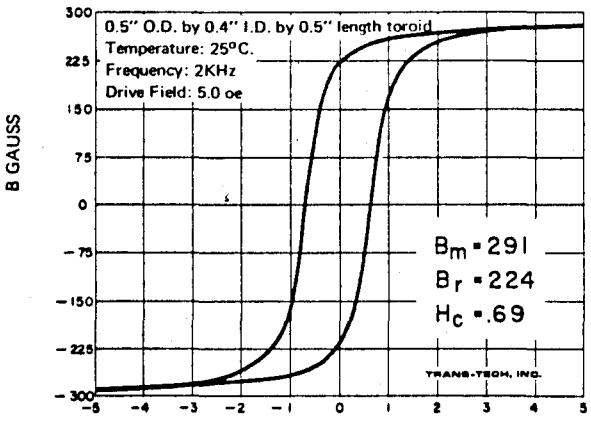

Hysteresis Loop for G-400

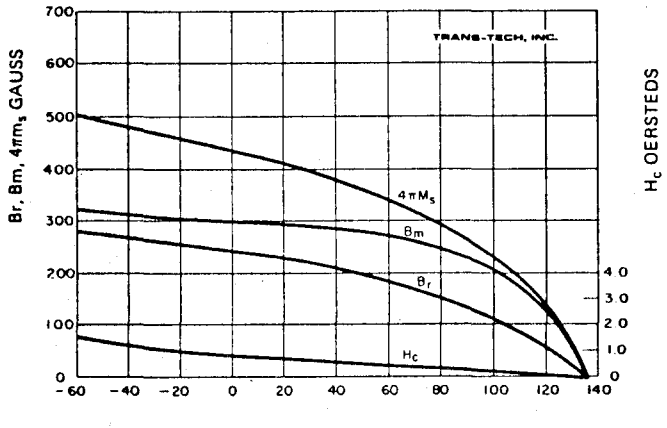

Temperature Variation of Hysteresis Loop Properties shown in adjacent graph and Saturation Magnetization for G-400

Specifications subject to change without notice.
Unless otherwise indicated, all data is nominal

AUGUST 1, 1972

12 MEEM AVENUE, GAITHERSBURG, MARYLAND/(301) 948-3800 TWX 710 828 0549

APPENDIX II

Fabrication of Phasers

The phasers produced for this thesis were of the Trans Tech G-400 material shown in Appendix I. The plates were 2x2x0.025 inches. These ferrite plates were very brittle and thus required ultrasonic drilling to make the required holes. To do this:

(1) 2x2x0.25 inch aluminum mounting blocks were produced, two for each device.

(2) The position of the holes for switching wiring were then drilled through the aluminum blocks.

(3) The OSM launchers were then mounted so that the two ferrite plates plus the centre conductor would fit between the two aluminum blocks.

(4) Next to each aluminum block, one of the ferrite plates was glued using 5 minute epoxy, and then a piece of two mil copper foil (thinnest foil available commercially) was glued using 5 minute epoxy to one of the plates.

(5) The centre conductors of the launchers were removed and the device was assembled,clamped and left to cure.

(6) After a minimum 24 hour curing period, holes were drilled through the ferrite plates plus centre conductor using the aluminum block holes as guides. These holes were approximately 1/8 inch in diameter.

(7) The next step in producing these devices is to disassemble and clean the copper foil using #3 Tripoli power.

(8) Then coat the aluminum block with a spray paint or some other protection against the ferric chloride etchant.

(9) Next etch the copper surface in ferrie cloride for one minute, then rinse in hydrochloric acid, then water, and allow to dry in air.

Note; do not heat the device in any way since the copper expands and bubbles, thus breaking the epoxy copper band.

(10) After the copper is thoroughly dry, mount on a spinner, deposit approximately 1/2 cc of Shipley's AZ-1350 positive photo resist (or equivalent) to the 2x2 inch copper surface and then spin until dry.

(11) Allow to stand in dark dust free space for an hour before photography

(12) When thoroughly dry, place mask over copper surface making sure that the circuit is close to the surface of the copper by weighting with glass plate if necessary. Expose from a distance of 18 inches with a Norelco PVY 650 watt, 120 volt projection lamp (or equivalent) for 2 minutes.

(13) Place exposed plate in 1% potassium hydroxide bath and agitate until all photo resist is removed from exposed areas.

(14) Rinse device in water and dry; then inspect under microscope and touch up any holes with some suitable paint or tar.

(15) Agitate in saturated ferric cloride bath at about 45^{o}C until exposed copper is removed and then remove remaining photo resist with acetone.

(16) Now mount device together making sure not to create undue stain on the ferrite plates. Ferrites are magnetostricture in nature and this

usually appears as a decrease in differential phase shift. It is essential that a shock and stress free mount be produced for any device that is to be used in other than laboratory conditions. (Referencce [7])

The preceding gives the technique used in producing the device. The author feels a few notes on difficulties encountered in attempting to produce this device are in order at this point.

The first attempts at producing these devices involved vacuum deposition techniques. In producing the ferrite plates, the material is firstly ground up and then polished to approximately 5 micron spheres. Then this powder is compressed and sintered into a solid of the mold's shape at between 1000 and 2000^{o}C. The result is a fairly porous ceramic, however, the exposed surface while appearing irregular under a microscope is really too smooth for a vacuum deposited metal to adhere to. To over come this, plates may be scrubbed with a coarse abrasive to create what the chemists call "dangling bonds". After removing any dust from the surface, the plate should be placed in a high vacuum (10^{-5} torr or better) and heated with no more than about a 15 watt heater for 2 or 3 days. This process will draw off as much moisture as is possible from the porous surface. After this the device should be allowed to cool while still under vacuum. After several hours of cooling (this time is necessary since all heat loss must occur by heat piping through the vacuum chamber mounting and by radiation), a slow vapour deposition of the metal may be begun. The process should be relatively slow (say 1KÅ^{o} per minute) so as not to create excessive localized heating on the surface which tends to boil off remaining moisture thus breaking the ferrite-aluminum bond.

Using the above technique, it is possible to deposit aluminum on ferrite and have a fairly good bond. However, it is not good enough to hold copper. Putting down a strike of 200Å of chromium and then copper works well also. The limitations to these techniques are in the available deposition units at McMaster. The various Edward's units can only lay down a maximum of 20,000 Å which is approximately one skin depth.

Attempts were made to electroplate copper which resulted in the copper separating from the chromium strike. The electro chemical potential of aluminum is below that of hydrogen so that electro-plating aluminum in a aquious solution results in the production of hydrogen chloride gas.

Attempts were made to make successive vacuum depositions of aluminum and of copper which resulted in layering of 20 KÅ deposits of metal separated by surface oxide films due to the exposure to air. Because at least five depositions were required to obtain five skin depths using this technique, invariably one of the layers would separate and peel off. Another possible reason for this was the temperature expansion coefficient of the metals.

What was really required was a source of metal vapour that would give a 100,000Å deposition and since this was not available, it was necessary to resort to the metal foil and adhesive technique.

REFERENCES

1. E.C. JORDAN and K.G. BALMAIN, "Electromagnetic Waves and Radiating Systems", 2nd ed., Prentice-Hall Inc., Englewood Cliffs, New Jersey, 1950, 1968.
2. S. CHIKAZUMI, "Physics of Magnetism", John Wiley and Sons, Inc., New York, N.Y., 1966.
3. J. HELSZAJN, "Principles of Microwave Ferrite Engineering", John Wiley and Sons, London, England, 1969.
4. G.T. ROOME and H.A. HAIR, "Thin Ferrite Devices for Microwave Integrated Circuits", IEEE Trans. Microwave Theory Tech., vol. MTT-16, pp. 411-420, July 1968.
5. T.S. SAAD, "Microwave Engineers Handbook, Volume 1", Artech House Inc., Dedham, Massachusetts, 1971.
6. L. MAYNARD, "Private Communication", Communications Research Centre, Ottawa, Canada, 1973.
7. R. EPSTEIN et al, "Magnetostriction Effects on Ferrite Material Parameters of Importance in Remanence Devices", IEEE Trans. Microwave Theory Tech., vol. MTT-16, January, 1968.
8. IEEE TRANS. MICROWAVE THEORY TECH.,"Special Issue on Microwave Control Devices for Array Antennas", vol. MTT-22, June, 1974.
9. L. R. WHICKER, "Ferrite Control Components,Vol. 1&2", Artech House, Dedham, Mass., 1974.
10. V. CROWE, "PIN Diode Phase Shifters", M. Eng. Thesis, McMaster University Hamilton, Ontario, Canada, 1974.

11. OLIVER and KNITTEL, "Phased Array Antennas", Artech House, Dedham, Mass., 1972.

12. B. LAX and K. J. BUTTON, "Microwave Ferrites and Ferrimagnetics ", McGraw Hill, New York, N.Y., 1962.

13. W. H. VON AULOCK and C. E. FAY, "Linear Ferrite Devices for Microwave Applications", Advances in Electronics and Electron Physics, Supplement 5, Academic Press, New York, N.Y., 1968.